Article

Using the LabVIEW Simulation Program to Design and Determine the Characteristics of Amplifiers

Corina Cuntan, Caius Panoiu *, Manuela Panoiu, Ioan Baciu and Sergiu Mezinescu

Department of Electrical Engineering and Industrial Informatics, University Polytechnica Timisoara, 300006 Timisoara, Romania; corina.cuntan@fih.upt.ro (C.C.); manuela.panoiu@fih.upt.ro (M.P.); ioan.baciu@fih.upt.ro (I.B.); sergiu.mezinescu@gmail.com (S.M.)
* Correspondence: caius.panoiu@fih.upt.ro; Tel.: +40-741012314

Abstract: Because of the large number of parameters that interact in amplifier functions, determining dynamic regime parameters as well as the mode of function of amplifier stages is an extremely complex problem. This paper describes a LabVIEW application for studying the functioning of an amplifier in various connections. The user selects the generator's parameters, the type of connection and its parameters, as well as the load circuit characteristics. The application can determine both the stage characteristics and the Bode characteristics. The amplifier's stability zone, as well as its gain and phase, are determined based on these characteristics. An important advantage of this application is that the design of the amplifier stage can be created starting from some parameters that the amplifier can establish, from which the values of components can be determined. In order to validate the simulation results from the LabVIEW application, the specialized program Multisim was used, as well as experimental measurements using the Electronics Explorer Board. Both Multisim and Electronics Explorer Board can determine Bode characteristics. In both simulations and experimental amplifiers, the same schemes with the same transistor were used. The application can be used for educational purposes as well as to design an amplifier's stage to achieve specific parameters.

Keywords: amplifier stage; dynamic regime parameters; Bode characteristics; gain and phase

1. Introduction

Although amplifiers are useful on their own, the design of an amplifier allows for the evaluation of various circuit design and analysis methods. When designing an amplifier, circuit design and PCB architecture should always consider amplifier stability. However, there are times when an amplifier is pushed to its absolute limit and fails to perform as expected, resulting in output signal distortion. Several publications in specialized journals investigate amplifier stability [1–3].

A variety of criteria, including Bode, are used to assess amplifier stability [1,4].

Because amplifier stability is a complex problem, many mathematical modelling methods have been developed to investigate it [2]. A computer tool that enables the mathematical examination of the physical stability of the bipolar transistor in the design of amplifiers is described in [2]. Users can set values for voltage gain, output impedance, input impedance, transistor current gain, and power supply current gain, and the software will return resistance values as a result. The study concluded that the power wasted in a bipolar transistor amplifier is inversely related to the magnitude of the input signal and directly proportional to the distance of half of the input signal from the operating point. It was determined that the operation point should be located higher than 0.05 and lower than 0.95, with 90% of the load line used for amplification.

In our study, we used LabVIEW myRIO 2014 software to simulate various amplifier types. This program is useful and appropriate for simulating analogue electronic circuits [5].

Other software programs for modelling electronic circuits are described in specialized literature. Multisim simulation software is one example [6]. Multisim was used to study

an amplifier used as a second order filter in [6]. Multisim 13 software can be used to create a circuit with inputs and outputs. Multisim was used in [6] to simulate a Bode plotter component and generate a frequency signal graph. A Bode plotter simplifies the examination of circuits, signal magnitude, and phase shape, and it can compare variations between circuits.

In [7], amplifiers were analysed using another software package, this time one written in Java. The software presented in [7] is a learning tool that enhances understanding of multi-stage amplifiers. This makes it possible for it to serve as a virtual guide with a user-friendly graphical interface that facilitates learning.

Several publications have proposed the common emitter (CE) amplifier design as a method for obtaining suitable amplifier performance parameters. The authors of [3] presented an amplifier that would perform well for devices that operate at low frequencies. The PSPICE program was used to research the proposed amplifier in [3,8]. For the investigation of amplifiers, the PSPICE program is useful. This bipolar junction transistor SPICE model from [8] was created to help students better understand amplifier design and analysis methods.

Because there is a need in technology to amplify electrical signals, i.e., to obtain on a load circuit higher power signals that are identical in terms of time variation to those of low power available, amplifiers are used [9–14]. Electronic amplifiers are constructed using bipolar or field effect transistors, either as discrete circuits or as integrated circuits.

In practice, there is a wide range of amplifiers. Their classification can be performed using a variety of criteria [15].

According to the frequency range of the amplified signals, there are direct current amplifiers, where the lower limit of the frequency of the amplified signal is 0 Hz; low frequency amplifiers, where the frequency band is in the range n × 10 Hz ÷ n × 10 kHz; broadband amplifiers, where the frequency band can be in the range 0 Hz ÷ n × 10 MHz; and narrowband amplifiers, in which the ratio between the maximum and minimum frequency of the signal to be processed is that of the order units.

According to the amplitude of the signal applied to the input, there are small signal amplifiers, where the amplitude of the input signal is small enough for the static operating point of the transistor to remain in a linear region of the dynamic or transfer characteristic, and large signal amplifiers, where the amplitude of the input signal is large enough for the static operating point of the transistor to remain in a linear region of the dynamic or transfer characteristic at which the amplitude of the input signal exits the linear region of the dynamic or transfer characteristic.

In dynamic mode, there are three types of connections made by the terminal of the bipolar transistor that are common at the input and output: common emitter connection, common collector connection, and common base connection.

According to the operating regime of the transistor, materialized by the conduction duration during a period of the signal, the amplifiers can operate in class A, where there is collector current throughout the period of the input signal; class B, where the current collector exists only on one half-period of the input signal; class C, where the transistor conducts less than one half-period of the input signal; and class AB, which represents an intermediate category between classes A and B.

According to the type of coupling between stages, there are amplifiers with direct coupling, capacitive coupling, transformer coupling, optical coupling, and so on.

The following main characteristics are used to evaluate and compare amplifier quality [15,16]: amplification, linear distortions such as frequency distortions, phase distortions, and transient distortions, nonlinear distortions, and noises.

The main characteristics of an amplification stage can be determined using the transistor's quadrupole parameters: current amplification, voltage amplification, input impedance or resistance, and output impedance or resistance. In this regard, the quadrupole parameters selected based on the frequency of the input signal can be used. For low frequencies, the parameters "h" (considered in this paper to have real values), "π" or "r" are partic-

ularly useful. For high frequencies, the parameters "y" or the natural equivalent circuit parameters "g" are used [15–18].

Because the functioning of amplification stages with bipolar transistors at low and medium frequencies was studied in this paper, the quadrupole "h" parameters, which are valid for any type of transistor connection, were taken into account.

Figure 1 depicts an equivalent circuit of an amplifier stage with a bipolar transistor using the quadrupole parameters "h" [15].
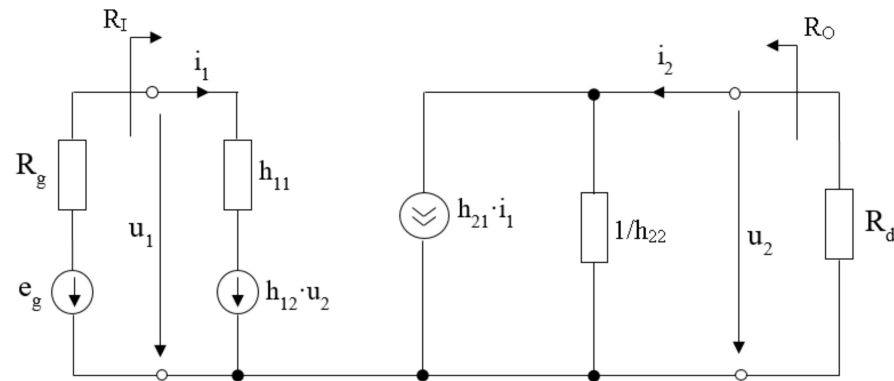

Figure 1. An equivalent circuit of an amplifier stage using the quadrupole "h" parameters.

The transistor's quadrupole equations are given by relation (1).

$$\begin{aligned} u_1 &= h_{11} \cdot i_1 + h_{12} \cdot u_2 \\ i_2 &= h_{21} \cdot i_1 + h_{22} \cdot u_2 \end{aligned} \tag{1}$$

For typical values of quadrupole "*h*" parameters, the second therm of each equation is significantly smaller than the first [4,5]. Under these situations, computing errors that are generated by neglecting these therms are smaller than the computing errors caused by component tolerances. Based on this finding, the typical values of the quadrupole parameters h_{12} and h_{22} had no substantial influence on the values of an amplifier's key features; hence, they were omitted in the application.

The effects of capacitor coupling between the signal generator and the amplifier, as well as between the amplifier and the load circuit, are independent and are included in the amplification expression in conventional amplification schemes. These effects consist of each capacitor introducing a low cut pulsation into the Bode diagram. The use of a bipolar transistor in the scheme of an amplification stage, on the other hand, generates a high cut pulsation due to the transistor's parasitic capacitances [15].

The Bode diagrams' gain-pulsation and phase-pulsation can be used to study the behaviour of an amplifier while accounting for these pulsations. The use of these diagrams also provides the benefit of determining the amplifier's stability area [15,16].

The amplifier that reflected the gain-pulsation and phase-pulsation characteristics has a single amplification stage. Common emitter, common collector, and common base connections were all considered. In the case of each connection, the values of the elements in the diagram can be selected and used to calculate the parameters of the amplification stages [14–16]. The values of the signal generator and load circuit elements, as well as the coupling elements, will be determined.

The paper is structured as follows: The first section discusses the challenges involved in designing an educational LabVIEW myRIO 2014 software application for studying the operation of an amplifier in various connections. In addition, this section includes works linked to this research subject. Section 2 determines the amplification characteristics of the stages in various connections, such as the common emitter, collector, and base connection. Section 3: The presentation of LabVIEW-implemented applications as a description of the software that was created using the relations outlined in Section 2. Section 4: Results of

simulation and experimentation via a comparison between the simulation results realised with our proposed software application, simulation results realised with Multisim, and experimental results. Section 5 provides research conclusions.

The goal of this work is to present a strategy for designing an amplifier's stage to attain particular parameters and to investigate the resulting performance. This application can be used for both research and instructional purposes.

2. Determination of the Amplifying Parameters of the Stages in Various Connections

The stage amplifier parameters in common emitter, common collector and common base connections will be determined in this section.

2.1. Common Emitter Connection

The main issue concerning common emitter connections will be presented in this paragraph [19–23]. Figure 2 shows the electronic scheme.
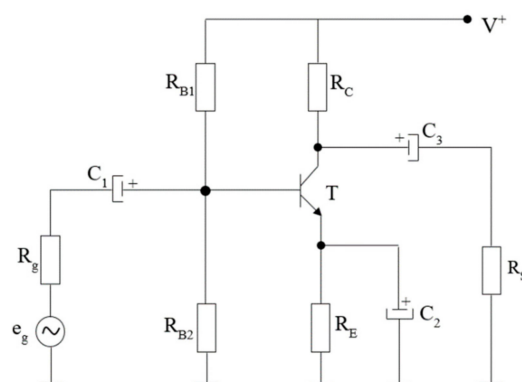

Figure 2. Electronic scheme for common emitter connection.

In this figure, capacitor C_2, if connected in the scheme, is a by-pass capacitor of resistance R_E. Because of the extremely low achievable impedance, the value of R_E that is taken into consideration during the simulation process if capacitor C_2 is utilized can be chosen from the application front panel. Alternatively, it can be left at 0. We assume that R_E holds the value introduced from the application's front panel if C_2 is not used in the simulation. This fact leads one to believe that in simulations, R_E has the value given by (2).

$$R_E \leftarrow \begin{cases} R_E \ or \ 0 & with \ C_2 \\ R_E & without \ C_2 \end{cases} \tag{2}$$

Two cases were studied in terms of equivalent resistance from the transistor's base. In the first case, assume that both R_{B1} and R_{B2} are present in the scheme, implying that the transistor polarization is with a resistive divider in the base. In the second case, assume that only R_{B1} is present in the scheme, implying that the transistor is polarized with resistance in the base. Both scenarios are taken into account during the simulation process.

Figure 3 depicts the equivalent scheme in the dynamical regime for a common emitter connection.

For both cases presented above, the determination of the input resistance in dynamical regime, Ri, of the common emitter connection is based on relations (3) and (4).

$$R_i = R_{B1} \| R_{B2} \| [h_{11e} + (1 + h_{21e}) R_E] \text{ with resistive divider in base} \tag{3}$$

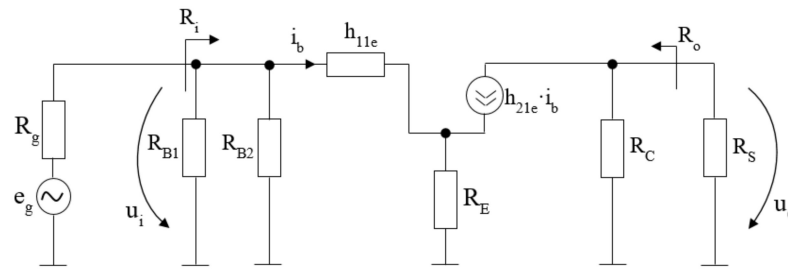$$R_i = R_{B1} \| [h_{11e} + (1 + h_{21e}) R_E] \text{ with resistance in base} \tag{4}$$

Figure 3. The equivalent scheme in dynamical regime for a common emitter connection.

Relation (5) made it possible to calculate the value of the output resistance, R_0, in a dynamical regime.

$$R_0 = R_C \tag{5}$$

Relation (6) can be used to calculate the value of voltage amplification, A_u.

$$A_u = -\frac{h_{21e} \cdot (R_c \| R_s)}{h_{11e} + (1 + h_{21e})R_E} \tag{6}$$

In relation (6), the dynamical parameters of the used transistor are the input impedance, h_{11e}, and amplification factor, h_{21e}. The choice of load resistance Rs, as shown in relation (7), is dependent on whether the common emitter stage whose operation is being simulated is the final stage of a multiple stage amplifier or not.

$$R_S \leftarrow \begin{cases} R_s & if\ it\ is\ the\ final\ stage \\ R_{IN} & if\ isn't\ final\ stage \end{cases} \tag{7}$$

2.2. Common Collector Connection

The main issue concerning common collector connections will be presented in this paragraph [15,16]. Figure 4 shows the electronic scheme.
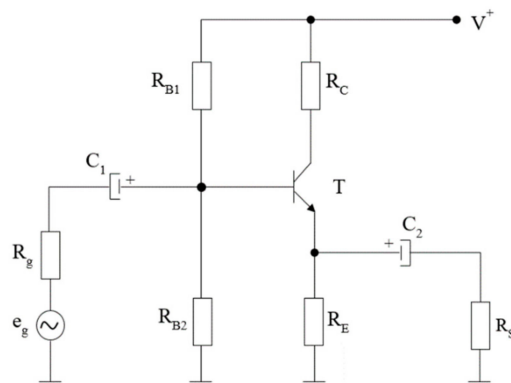

Figure 4. Electronic scheme for a common collector connection.

In terms of equivalent resistance from the transistor's base, the same two cases were studied as in the common emitter connection in terms of the presence of R_{B1} and R_{B2} resistance. Both scenarios are taken into account during the simulation process.

Figure 5 depicts the equivalent scheme in the dynamical regime for a common collector connection.

For both cases presented previously, the determination of the input resistance in dynamical regime, R_i, for a common collector connection is based on Relations (8) and (9).

$$R_i = R_{B1} \| R_{B2} \| [h_{11c} + (1 + h_{21c}) \cdot R_E \| R_S]\ \text{with resistive divider in base} \tag{8}$$

$$R_i = R_{B1} \| [h_{11c} + (1 + h_{21c})R_E]\ \text{with resistance in base} \tag{9}$$
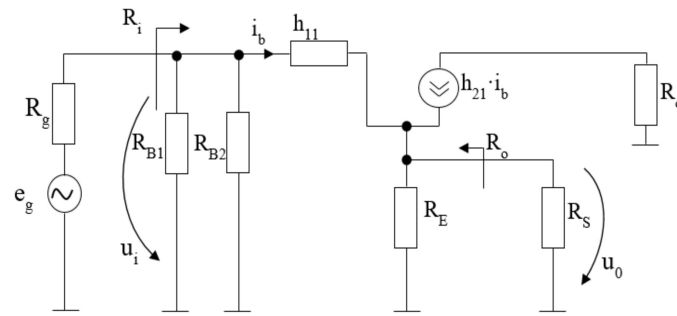
Figure 5. The equivalent scheme in dynamical regime for a common collector connection.

The determination of the output resistance in dynamical regime, R_0, of the common collector connection is based on Relations (10) and (11) for both cases presented previously.

$$R_0 = R_E \| [h_{11c} + R_{B1} \| R_{B2} \| R_G] / (1 + h_{21c}) \text{ if the first stage is with resistive divider in base} \tag{10}$$

$$R_0 = R_E \| [h_{11c} + R_{B1} \| R_G] / (1 + h_{21c}) \text{ if the first stage is with resistance in base} \tag{11}$$

The choice of generator resistance R_G, as shown in Relation (12), is determined by whether or not the common collector stage whose operation is being simulated is the first stage of a multiple stage amplifier.

$$R_G \leftarrow \begin{cases} R_G & if\ is\ the\ first\ stage \\ R_{0,\ prev} & if\ isn't\ first\ stage \end{cases} \tag{12}$$

Relation (13) can be used to calculate the value of voltage amplification, A_u.

$$A_u = \frac{u_0}{u_i} = \frac{(R_E \| R_S)(1 + h_{21c})}{h_{11c} + (R_E \| R_S)(1 + h_{21c})} \tag{13}$$

The dynamical parameters of the used transistor in Relation (13) are the input impedance, h_{11c}, and amplification factor, h_{21c}. The choice of load resistance Rs, as shown in Relation (14), is determined by whether or not the common collector stage whose operation is being simulated is the final stage of a multiple stage amplifier.

$$R_S \leftarrow \begin{cases} R_S & if\ is\ the\ final\ stage \\ R_{IN} & if\ isn't\ final\ stage \end{cases} \tag{14}$$

2.3. Common Base Connection

This paragraph will focus on the main issue of common base connections [15,21,22]. The electronic scheme is depicted in Figure 6.
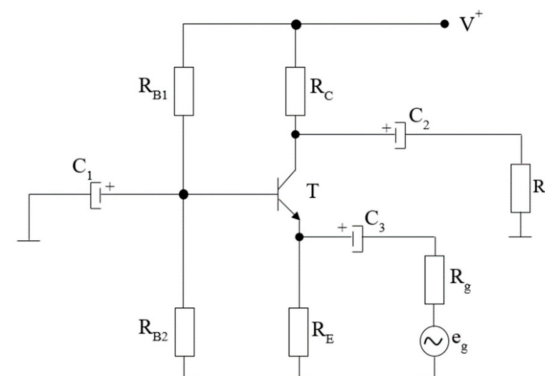

Figure 6. Electronic scheme for common base connection.

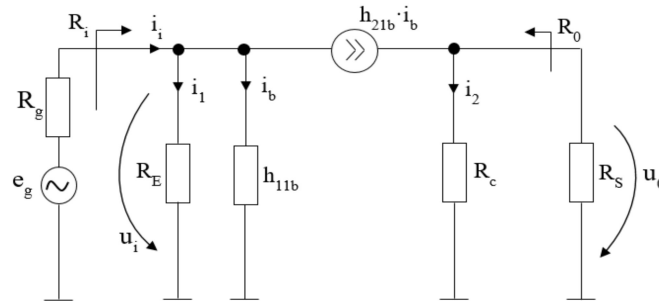Figure 7 depicts the dynamical equivalent scheme for a common base connection.

Figure 7. The equivalent scheme in dynamical regime for a common base connection.

In Relation (15), the determination of the input resistance, R_i, in the dynamical regime in a common base connection is presented. The dynamical parameters of the used transistor in Relation (15) are the input impedance, h_{11b}, and amplification factor, h_{21b}.

$$R_i = \frac{h_{11b} \cdot R_E}{h_{11b} + (1 + h_{21b}) R_E} \tag{15}$$

The value of the output resistance, R_0, in dynamical regime in the common base connection can be computed from Relation (16).

$$R_0 = R_C \tag{16}$$

Relation (17) can be used to calculate the value of voltage amplification, A_u.

$$A_u = \frac{h_{21b} \cdot R_C \| R_S}{h_{11b}} \tag{17}$$

The choice of load resistance R_s, as shown in Relation (18), is determined by whether or not the common base stage whose operation is being simulated is the final stage of a multiple stage amplifier.

$$R_S = \begin{cases} R_S & \text{if is the final stage} \\ R_{IN} & \text{if isn't final stage} \end{cases} \tag{18}$$

3. Presentation of LabVIEW-Implemented Applications

Figure 8 depicts the main application, which is a study of an amplifier using bipolar transistors [15]. The application is intended to use an amplifier with three stages, but this paper focuses on a situation with only one stage.

The number of stages can be selected in the left-upper part of Figure 8, which in this case contains only one stage. In the left section, there are also five control buttons that allow the selection of the amplifier's input/output parameters, one of three amplifier stages, and finally a representation of the Bode diagram [24–27].

3.1. Input/Output Parameters

The "Input/output parameters" menu is depicted in Figure 8. This menu displays the equivalent scheme for the case where there is only one amplifier stage, as well as the relationships that allow voltage amplification to be calculated.

This menu allows you to select values for generator parameters, R_g and e_g, load resistance, Rs, and coupling capacitors between the generator and the amplifier stage, C_G, as well as the amplifier stage and the load, Cs.

In this figure, the parameters of the amplifier stage that is connected to the generator are also shown: input resistance, R_{i1}, output resistance, R_{o1}, and voltage amplification, A_{u1}.
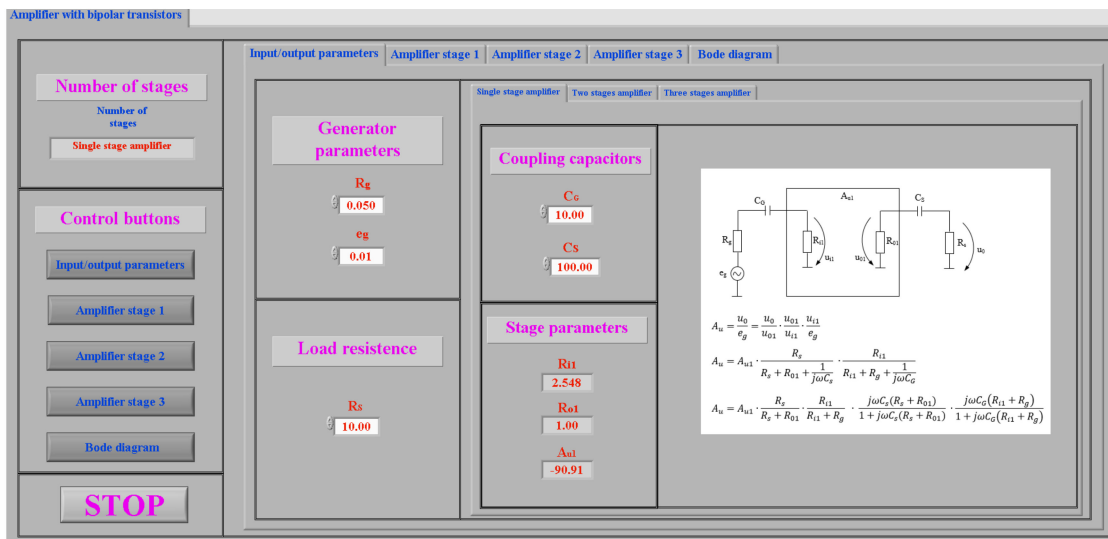
Figure 8. Front panel for input/output parameters.

3.2. Implementation of the Presented Connections in LabVIEW

The implementation of all three connections will be presented in this section. For each connection, the front panel and the role of each element, as well as the programming panel, will be described [28–30].

3.2.1. Implementation of an Amplifier Stage with a Common Emitter Connection

Figure 9 depicts the "Common emitter" menu [20,22]. This menu displays the amplifier stage's scheme, as well as an option to view the dynamic regime diagram shown in Figure 10a, and the dynamic parameters for a common emitter connection shown in Figure 10b.

Users can select settings for common emitter stage input characteristics including base resistances R_{B1e1} and R_{B2e1}, collector resistance R_{Ce1}, emitter resistance R_{Ee1}, and dynamic regime parameters like input impedance, h_{11e1}, and amplification factor h_{21e1}. The high cutting frequency of the used transistor can be set from F_{Tei1} using the data sheet transistor parameters.

The switch "SW_{RSe1}" selects the value of R_S from Relation (6) according to Relation (7), in the context of calculating stage voltage amplification.
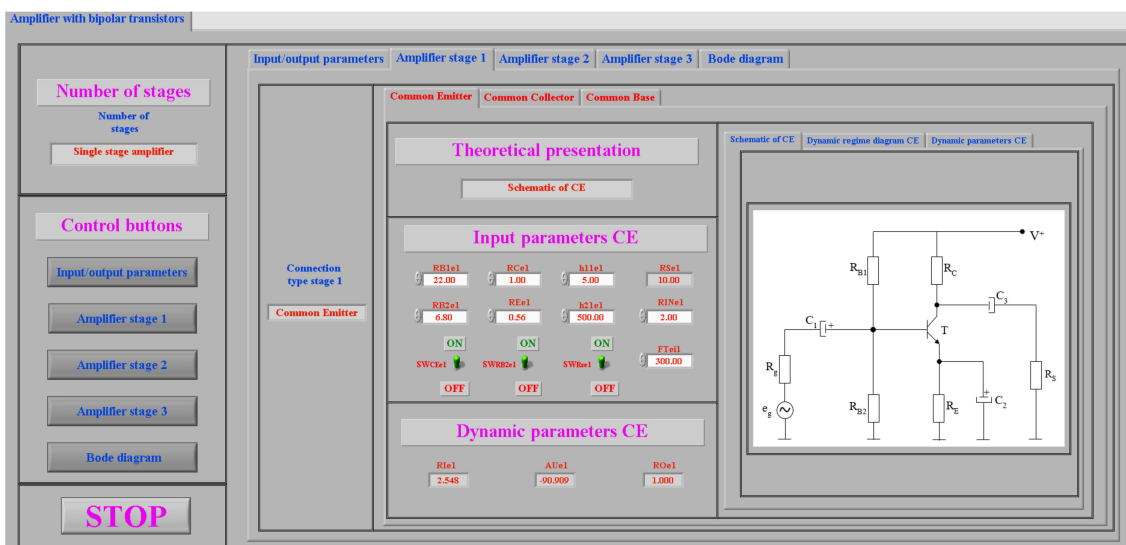

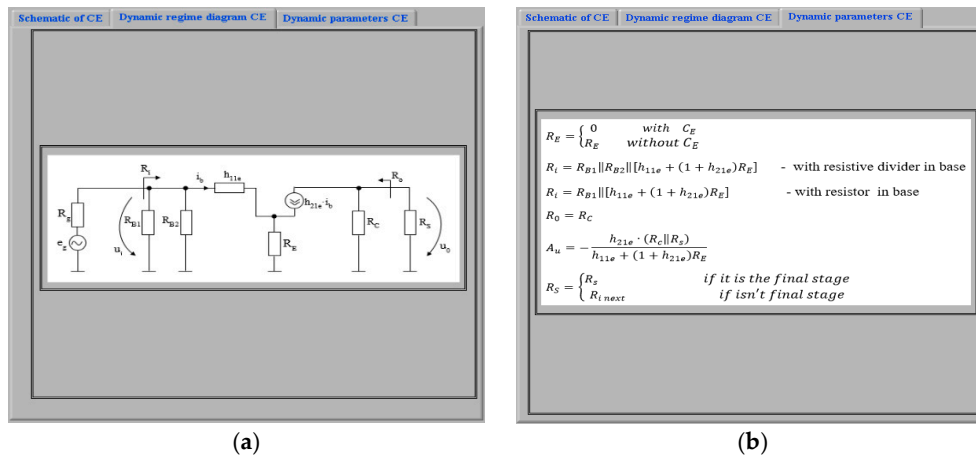**Figure 9.** Front panel for common emitter stage parameters.

Figure 10. (**a**) Dynamic regime diagram CE, (**b**) Dynamic parameters CE.

The program allows the user to select the polarization mode of the transistor base with resistive divider or resistance in the base by using the switch "SW$_{RB2e1}$".

It is also possible to use the "SW$_{CEe1}$" switch to connect/disconnect the resistor from the emitter and observe the effect on the amplifier parameters.

The dynamic parameters of the amplifier stage are computed based on the values of the input parameters: input resistance, R$_{Ie1}$, output resistance, R$_{Oe1}$, and voltage amplification, A$_{ue1}$.

Figure 11a depicts the program's implementation of parameters computed for a common emitter connection. This program employs the "EC1" subroutine, shown in Figure 11b, which is used to compute the output parameters.
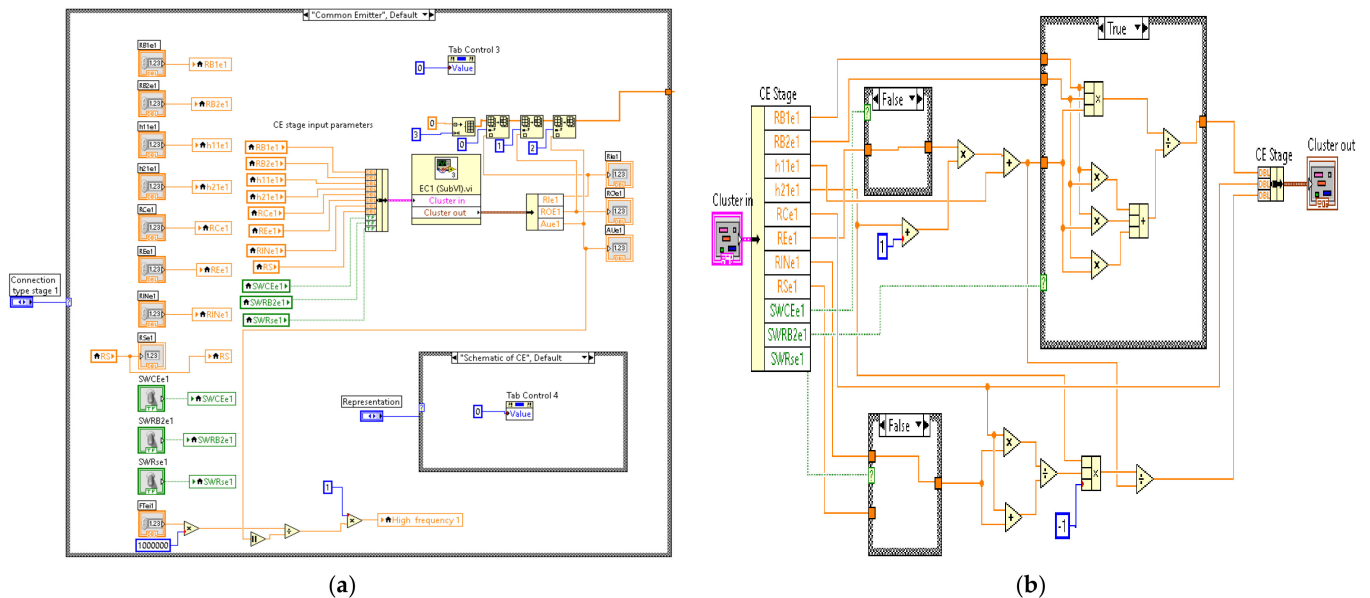

Figure 11. (**a**) Program implementation of computed parameters, (**b**) Subroutine EC1.

3.2.2. Implementation of an Amplifier Stage with a Common Collector Connection

Figure 12 depicts the "Common collector" menu. This menu displays the amplifier stage's scheme, as well as an option to view the dynamic regime diagram shown in Figure 13a, and the dynamic parameters for a common collector connection shown in Figure 13b.
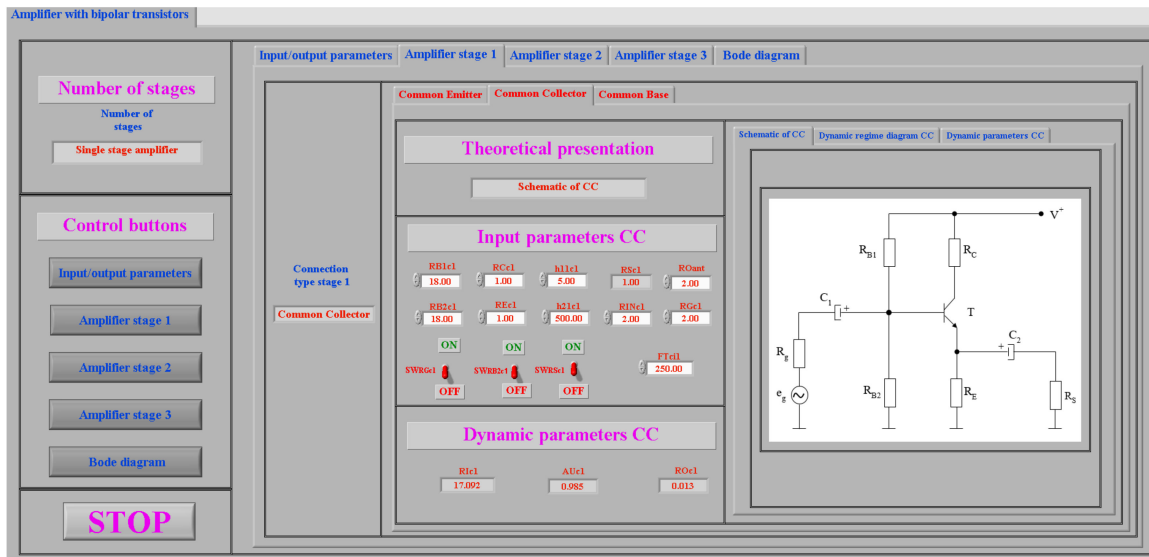
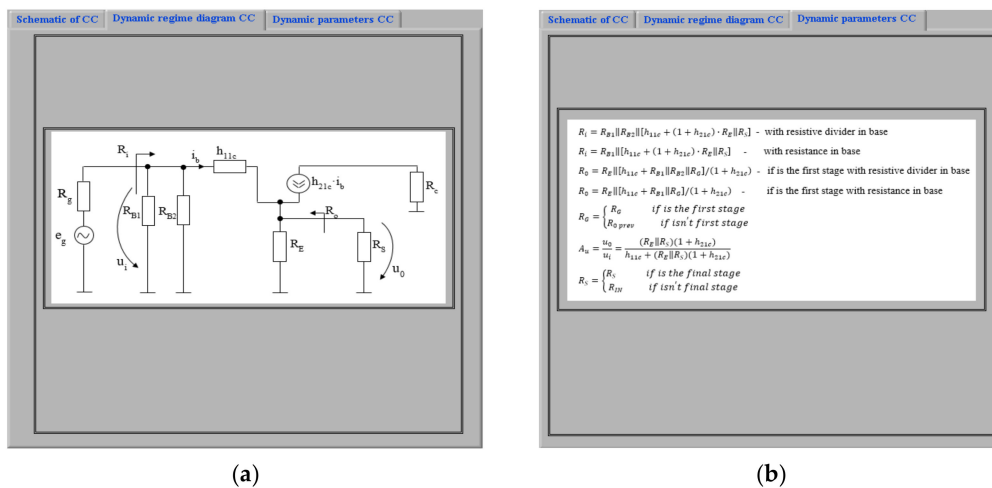**Figure 12.** Front panel for common collector stage parameters.

(**a**)   (**b**)

Figure 13. (**a**) Dynamic regime diagram CC, (**b**) Dynamic parameters CC.

Users can select settings for common collector stage input characteristics including base resistances R_{B1c1} and R_{B2c1}, collector resistance R_{Cc1}, emitter resistance R_{Ec1}, and dynamic regime parameters like input impedance, h_{11c1}, and amplification factor h_{21c1}. The high cutting frequency of the used transistor can be set from F_{Tci1} using the data sheet transistor parameters.

The switch "SW_{RSc1}" selects the value of R_S from Relation (13) according to Relation (14), in the context of calculating stage voltage amplification.

The program allows the user to select the polarization mode of the transistor base with resistive divider or resistance in the base by using the switch "SW_{RB2c}".

To compute the value of Ro according to Relations (10) and (11), the value of R_G can be selected as in (12) using the switch "SW_{RGc1}".

The dynamic parameters of the amplifier stage are computed based on the values of the input parameters: input resistance, R_{Ic1}, output resistance, R_{Oc1}, and voltage amplification, A_{uc1}.

Figure 14a depicts the program's implementation of parameters computed for a common collector connection. This program employs the "CC1" subroutine shown in Figure 14b, which is used to compute the output parameters.
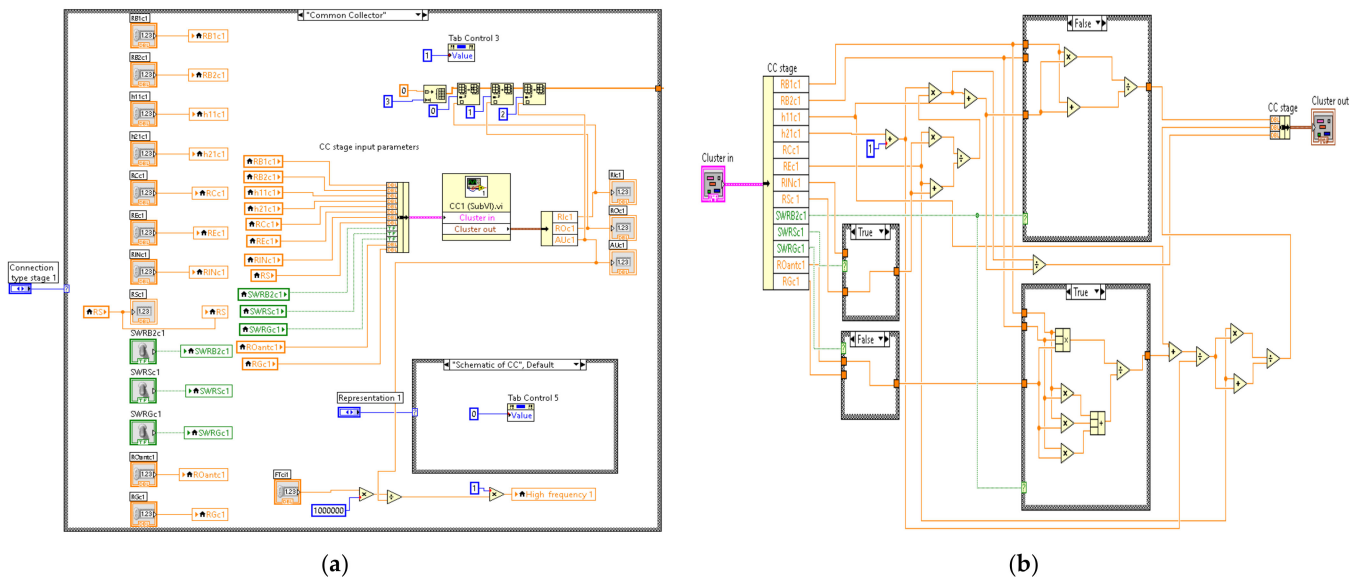
(**a**)   (**b**)

Figure 14. (**a**) Program implementation of computed parameters, (**b**) Subroutine CC1.

3.2.3. Implementation of an Amplifier Stage with a Common Base Connection

Figure 15 depicts the "Common base" menu [19,22]. This menu displays the amplifier stage's scheme, as well as an option to view the dynamic regime diagram shown in Figure 16a, and the dynamic parameters for a common base connection shown in Figure 16b.
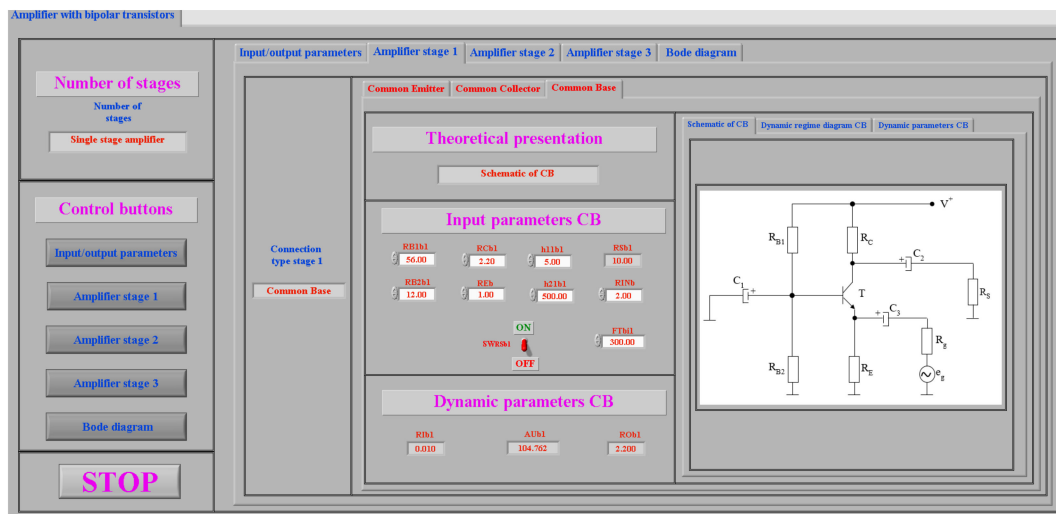

Figure 15. Front panel for common base stage parameters.

Users can select settings for common emitter stage input characteristics including base resistances R_{B1b1} and R_{B2b1}, collector resistance R_{Cb1}, emitter resistance R_{Eb1}, and dynamic regime parameters like input impedance, h_{11b1}, and amplification factor h_{21b1}. The high cutting frequency of the used transistor can be set from F_{Tbi1} using the data sheet transistor parameters.

The switch "SW_{RSb1}" selects the value of R_S from Relation (17) according to Relation (18), in the context of calculating stage voltage amplification.

The dynamic parameters of the amplifier stage are computed based on the values of the input parameters: input resistance, R_{Ib1}, output resistance, R_{Ob1}, and voltage amplification, A_{ub1}.
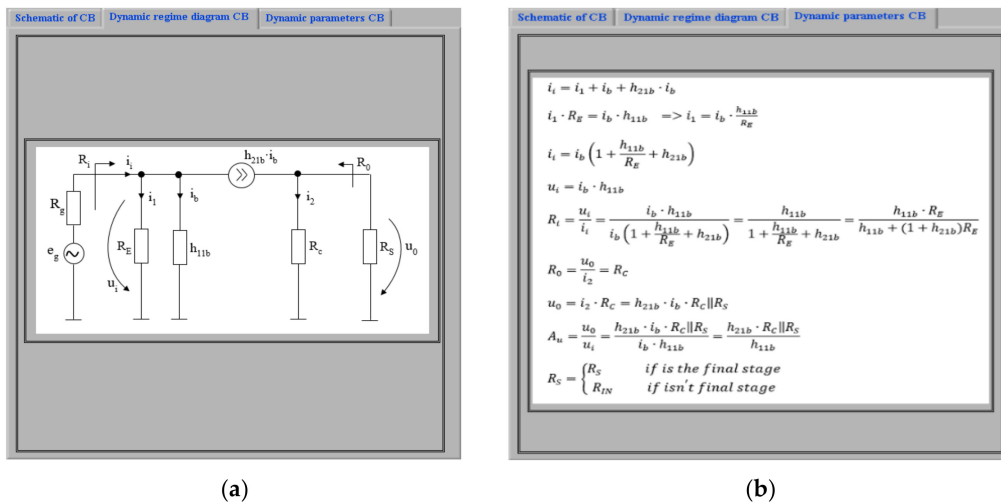
Figure 16. (**a**) Dynamic regime diagram CB, (**b**) Dynamic parameters CB.

Figure 17a depicts the program's implementation of parameters computed for a common base connection. This program employs the "BC1" subroutine shown in Figure 17b, which is used to compute the output parameters.
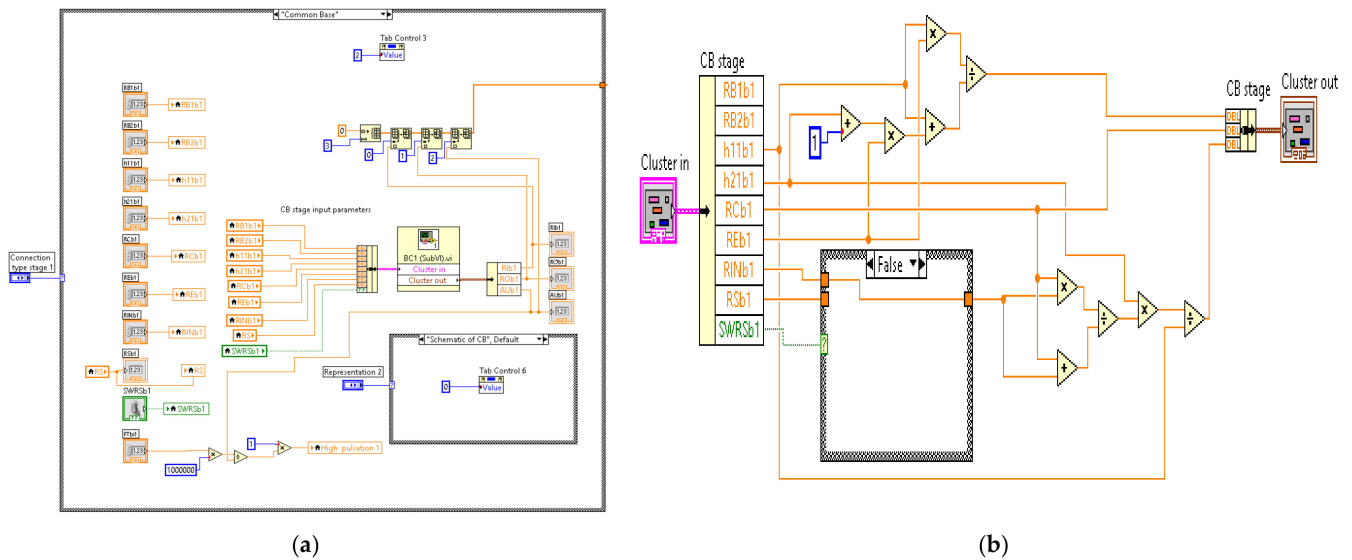

Figure 17. (**a**) Program implementation of computed parameters, (**b**) Subroutine BC1.

3.3. Computing and Implementation of Bode Diagram

Figure 18 depicts the "Bode diagram" menu, which can be accessed via the control button "Bode diagram" [24–27]. The characteristics "Gain-Frequency" and "Phase-Frequency" are represented in a semi-logarithmic scale on the right side of this menu (linear scales for gain and phase and logarithmical scale for frequency). The gain and phase dependency for the frequency choice domain are represented by white lines. The red line represents the stability domain, where the phase is between $-90°$ and $90°$. A green line represents the position of a specified point on the graphs.
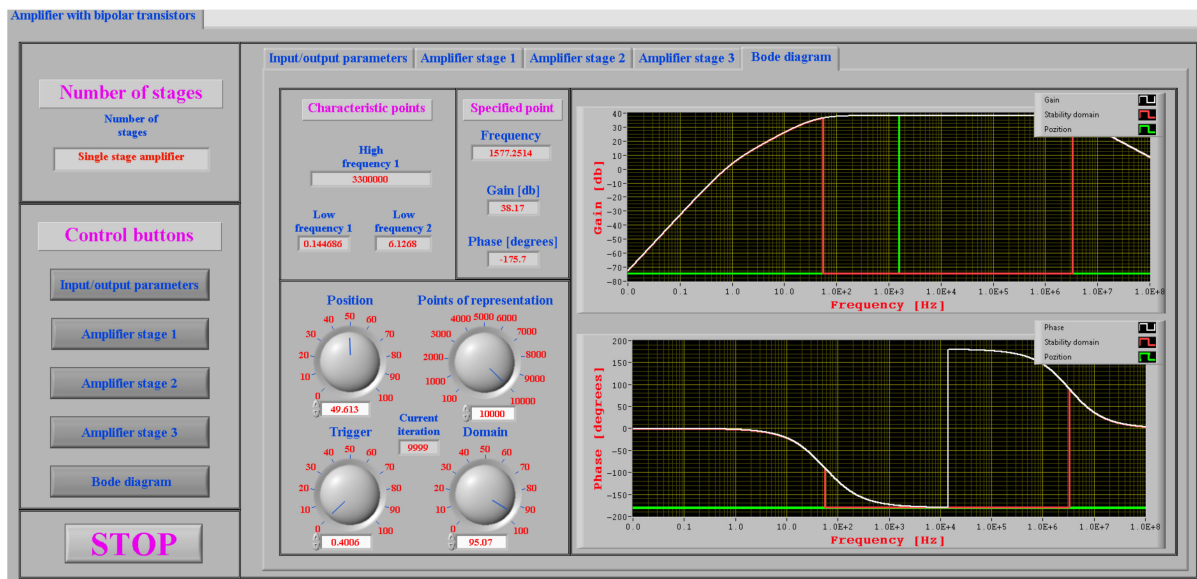
Figure 18. Bode diagram menu.

As seen from the gain-frequency characteristic, there are three characteristic points for a single stage of the amplifier. The first of them represents the high cutting frequency of the used transistor, which was set in the "Amplifier stage 1" menu in Figure 9. The next two characteristic points represent low cut frequencies, determined by C_G, R_{i1} and R_g for f_1, and C_S, R_{o1} and R_S for f_2, calculated using Relations (19) and (20).

$$f_1 = \frac{1}{2 \cdot \pi \cdot C_G \cdot (R_{i1} + R_g)} \tag{19}$$

$$f_2 = \frac{1}{2 \cdot \pi \cdot C_S \cdot (R_{o1} + R_S)} \tag{20}$$

According to Relations (21) and (22), the frequency domain is chosen to range from a minimum frequency f_{min} to a maximum frequency f_{max}, providing the possibility of representing all three characteristic points.

$$f_{min} = \frac{min\{f_1; f_2\}}{10} \tag{21}$$

$$f_{max} = 10 \cdot F_{Ti1} \tag{22}$$

To obtain the graphs in Figure 18, the application computes the gain and phase values into a number of points that can be selected from the "Points of representation" knob, which is located in the [100;10,000] domain. The graphic resolution of the diagrams is defined by the number of points represented, N. Because the frequency has a logarithmic representation, the distance between two consecutive points is defined in Relation (23).

$$\Delta_f = \frac{log(f_{max}) - log(f_{min})}{N - 1} \tag{23}$$

The starting point of the graphic representation can be set using the "Trigger" knob, which ranges from 0% to 100% of the full range of representation. The domain of representation can be selected from 0% to 100% of the total range of representation using the "Domain" knob.

The "Position" knob can be used to obtain information about a specific point. After selecting a specific point from the "Specific point" menu, information on frequency, gain, and phase can be obtained.

The program implementation of Bode diagrams for a single stage amplifier is shown in Figure 19.
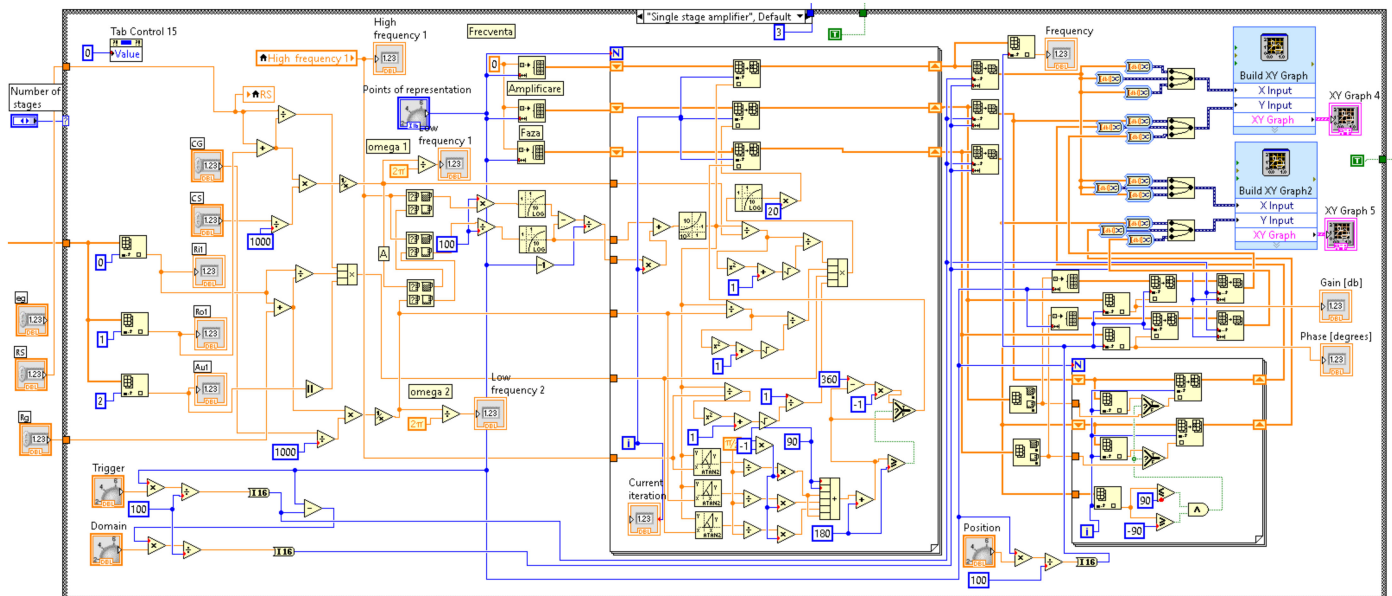

Figure 19. Program implementation of Bode diagram menu.

4. Results of Simulation and Experimentation

This section contains simulation and experimentation results for an amplifier operating in the connections presented in Section 2: common emitter, common collector, and common base [31–37].

In order to validate the simulation results using the LabVIEW application, the specialized program Multisim was used, as well as experimental measurements using the Electronics Explorer Board. Bode characteristics can be determined using both Multisim and the Electronics Explorer Board. The same transistor was used in both simulations and experimental amplifiers.

4.1. Simulation and Experimentation Results for Common Emitter Connection

The input parameter values for this connection were chosen in such a way that the Bode diagram presented two different low pulsations [15,16]. These values are: for generator parameters, R_g = 0.05 kΩ and e_g = 10 mV; for load resistance, Rs = 10 kΩ; for coupling capacitors between generator and amplifier stage, C_G = 10 μF; and for coupling capacitors between amplifier stage and load, Cs = 100 μF. As shown in Figures 9, 12 and 15, a BC 109 transistor with h_{11e} = 5 k, h_{21e} = 500, and f_T = 300 MHz was used in both simulations and experimental measurements. These parameter values correspond to data from the Data Sheet.

The parameter values for the common emitter connection are presented in Figure 9.

As previously stated, the structure of an amplifier stage can be modified using the switches SW_{CEe1}, SW_{RB2e1} and SW_{RSe1}. Table 1 present the values of the output parameters R_{Ie1}, A_{Ue1} and R_{Oe1} for all situations in which SW_{CEe1}, SW_{RB2e1} and SW_{RSe1} can be established.

Table 1. The values of the output parameters.

	SW$_{RB2e1}$	SW$_{RSe1}$	R$_{Ie1}$ [kΩ]	A$_{Ue1}$	R$_{Oe1}$ [kΩ]
OFF	OFF	OFF	20.426	−1.167	1.000
OFF	OFF	ON	20.426	−1.592	1.000
OFF	ON	OFF	5.102	−1.167	1.000
OFF	**ON**	**ON**	**5.102**	**−1.592**	**1.000**
ON	OFF	OFF	4.074	−66.667	1.000
ON	OFF	ON	4.074	−90.909	1.000
ON	ON	OFF	2.548	−66.667	1.000
ON	**ON**	**ON**	**2.548**	**−90.909**	**1.000**

Table 1 reveals some conclusions regarding the effect of the three switches on the values of the output parameters.

1. Connecting capacitor C$_2$ from Figure 20 with the switch SW$_{CEe1}$ in the ON state results in a significant increase in A$_{Ue1}$ and a decrease in R$_{Ie1}$.

2. Selecting the polarization mode of the transistor base with a resistive divider by connecting the switch SW$_{RB2e1}$ in the ON state causes the input resistance R$_{Ie1}$ to decrease.

3. Switching SW$_{RSe1}$ in the ON state is conducive to an increase in A$_{Ue1}$ of about 35%.

4. None of the three switches have any effect on the R$_{Oe1}$ value.

The effect of switch SW$_{CEe1}$ can be seen in the Bode diagrams in Figures 20–22 with SW$_{CEe1}$ to ON, line 8 from Table 1. All of these figures were obtained through simulations with the presented application and allow for the low and high cut frequency to be determined. These frequencies were determined as the points where the gain was reduced by 3 decibels.
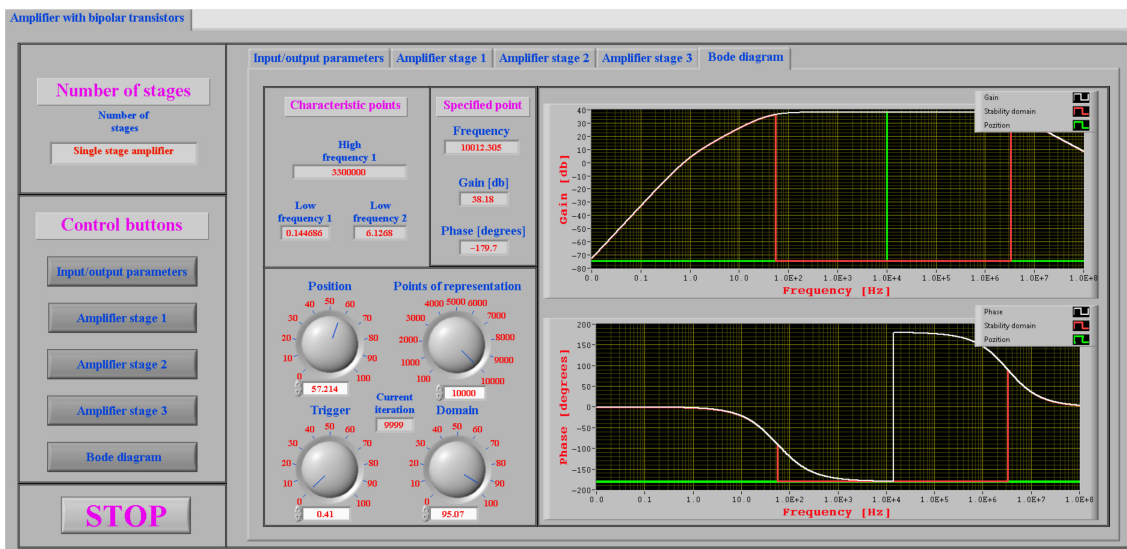

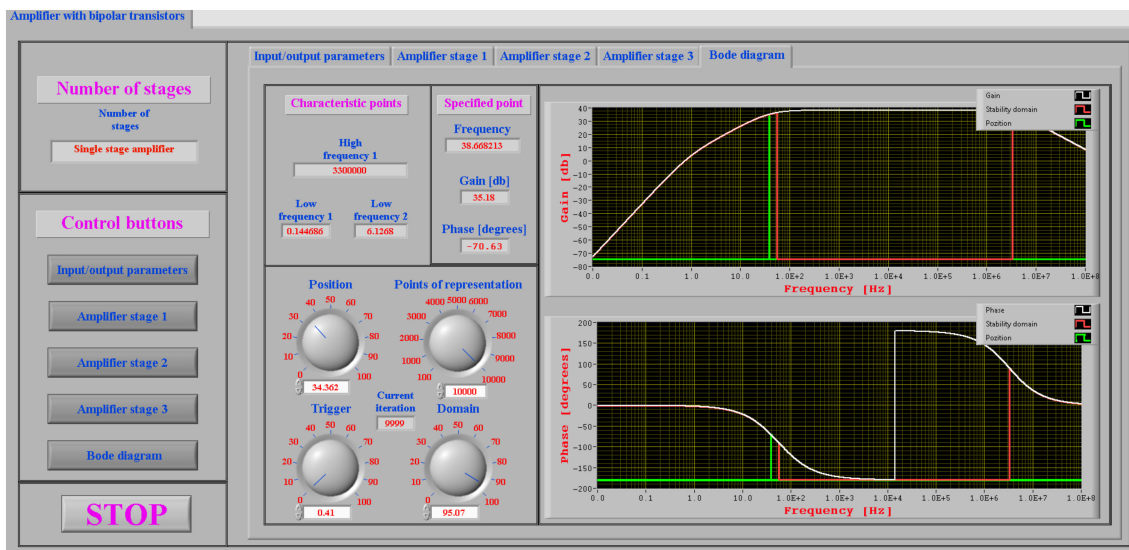**Figure 20.** Bode diagram for line 8 from Table 1 with SW$_{CEe1}$ to ON, for 10 kHz frequency.

Figure 21. Bode diagram for line 8 from Table 1 with SW$_{CEe1}$ to ON, for low cut frequency of 38.66 Hz.
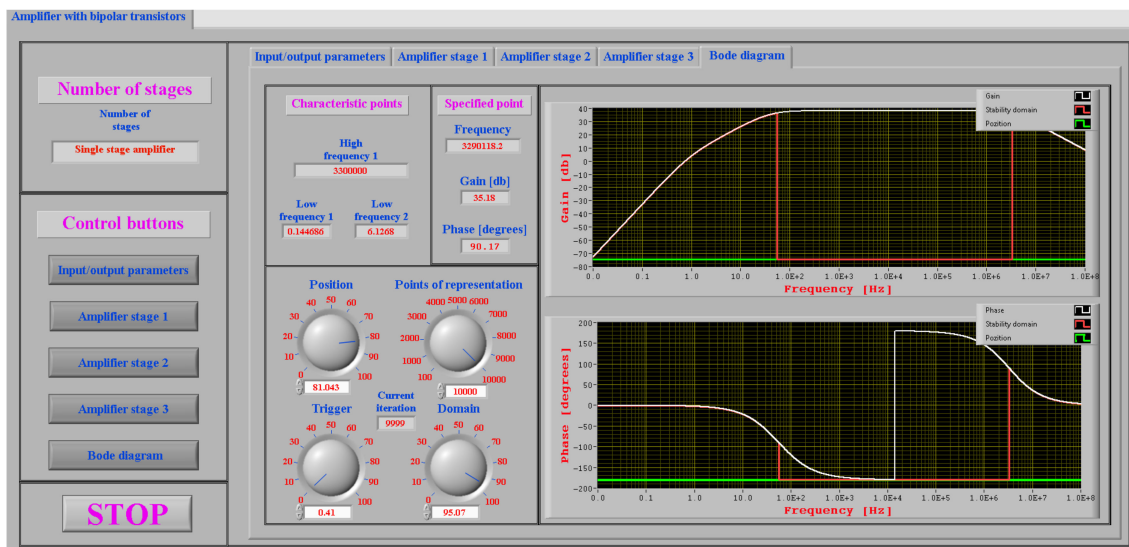

Figure 22. Bode diagram for line 8 from Table 1 with SW$_{CEe1}$ to ON, for high cut frequency of 3.29 MHz.

Multisim, a specialized simulation program, was used to verify the LabVIEW simulation results. The simulation results obtained with Multisim are shown in Figure 23.

In order to validate the simulation results produced by LabVIEW and Multisim, experimental measurements were performed on a real circuit using an Electronic Explorer Board, which can also be used to determine the Bode characteristics. The Electronic Explorer Board has a frequency range of up to 10 MHz.
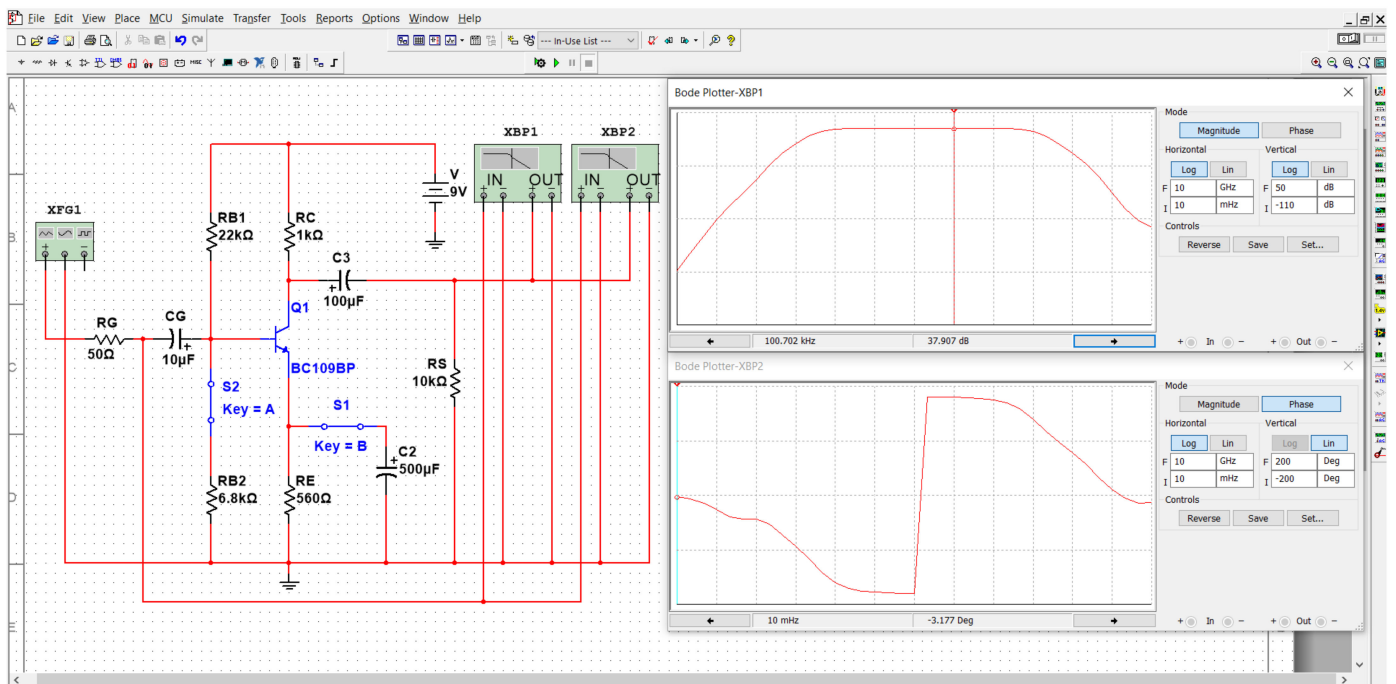
Figure 23. Simulation results for common emitter connection with SW$_{\text{CEe1}}$ to ON, using Multisim.

The measurement results obtained with the Electronic Explorer Board are presented in Figure 24.
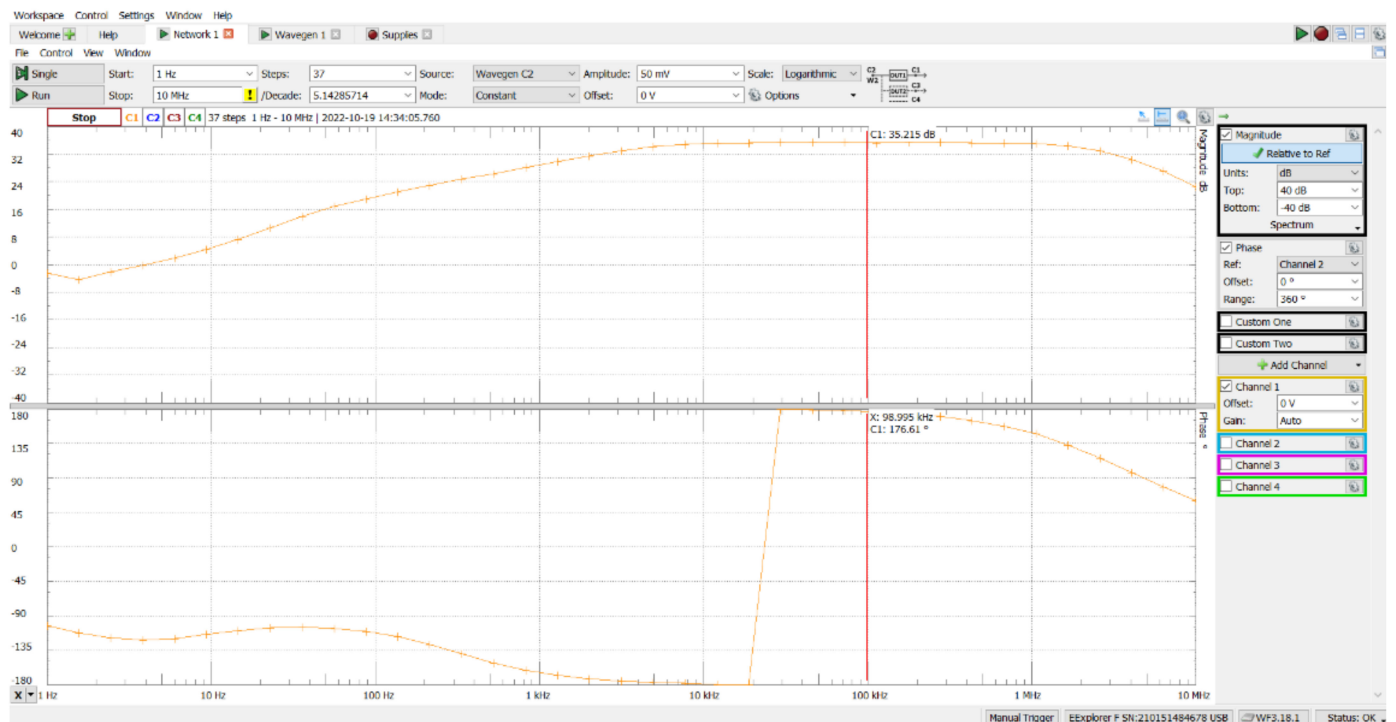

Figure 24. Measurement results for common emitter connection with SW$_{\text{CEe1}}$ to ON, using Electronic Explorer Board.

A comparison between the simulations and the experimental results can be seen in Figure 25.
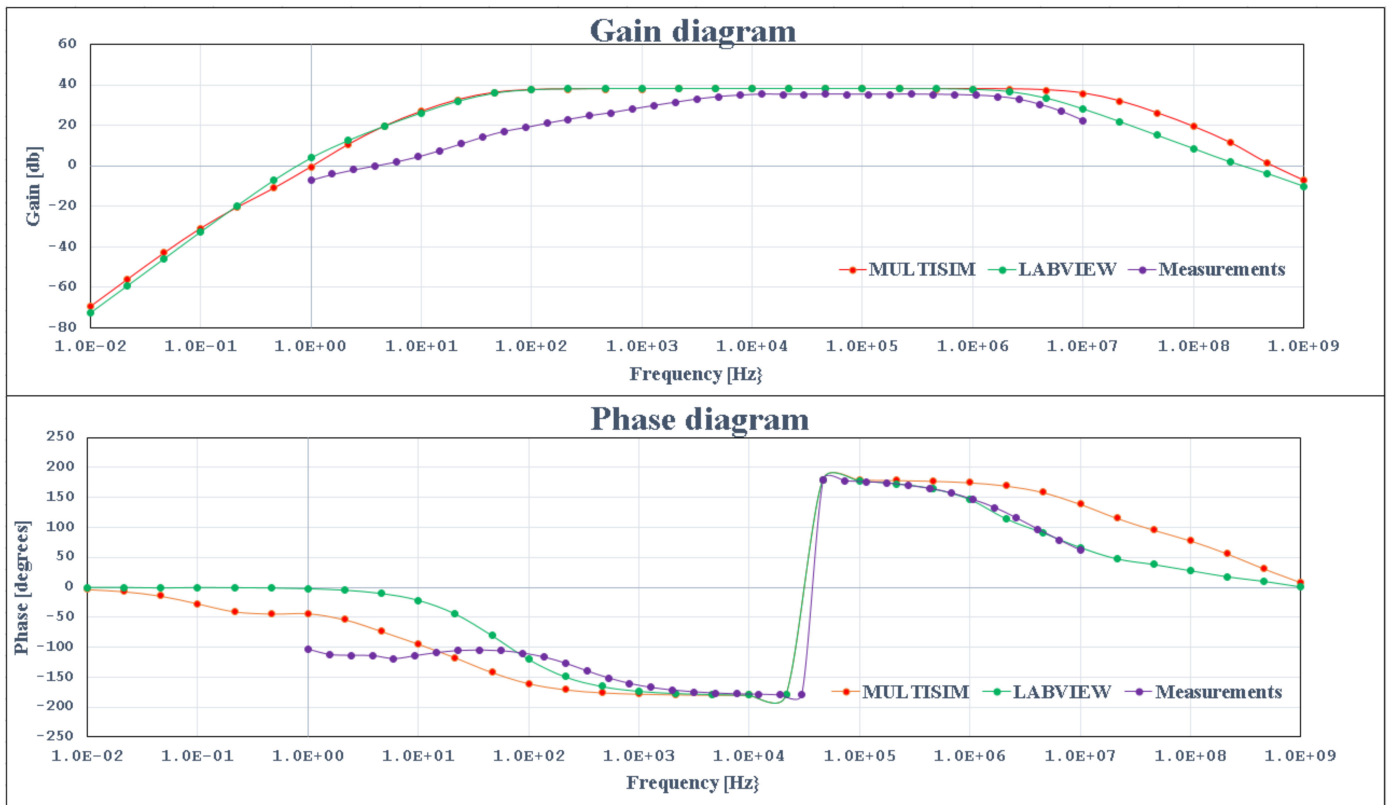
Figure 25. Simulations and experimental results for common emitter connection with SW$_{CEe1}$ to ON.

Analyzing the gain diagram reveals that the simulation and experimental results are very similar at medium and high frequencies. In terms of the phase diagram, both simulations and measurements achieve the same crossing from $-180°$ to $180°$, and the LabVIEW simulations and measured results are nearly identical at medium and high frequencies.

The effect of switch SW$_{CEe1}$ can be seen in the Bode diagrams in Figures 26–28 with SW$_{CEe1}$ to OFF, line 4 from Table 1.
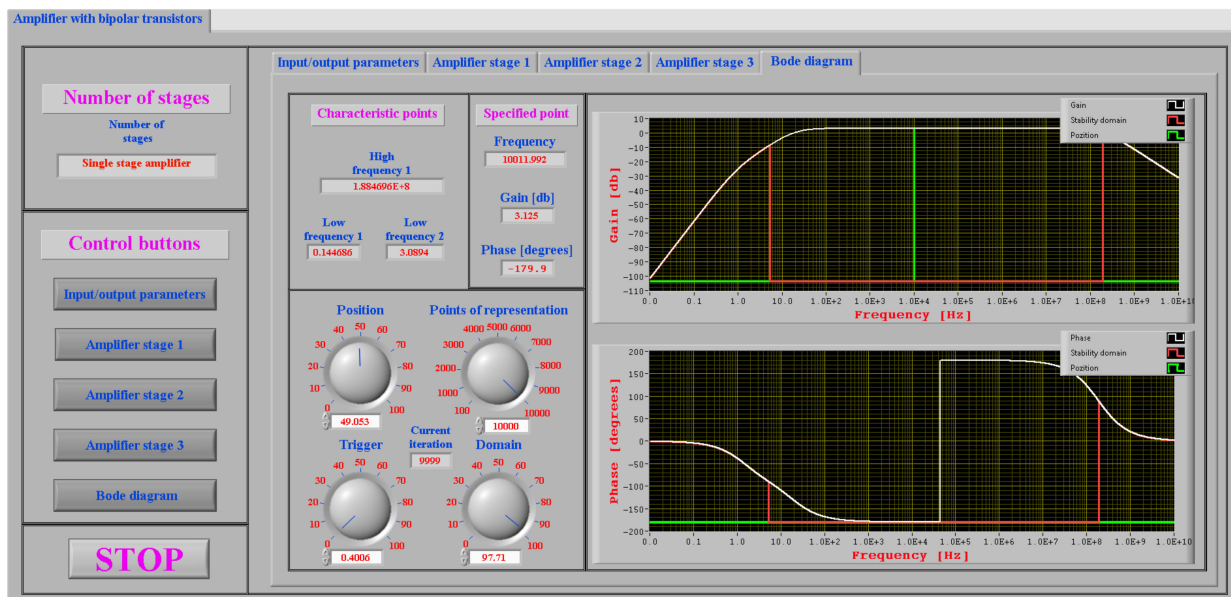

Figure 26. Bode diagram for line 4 from Table 1 with SW$_{CEe1}$ to OFF, for 10 kHz frequency.
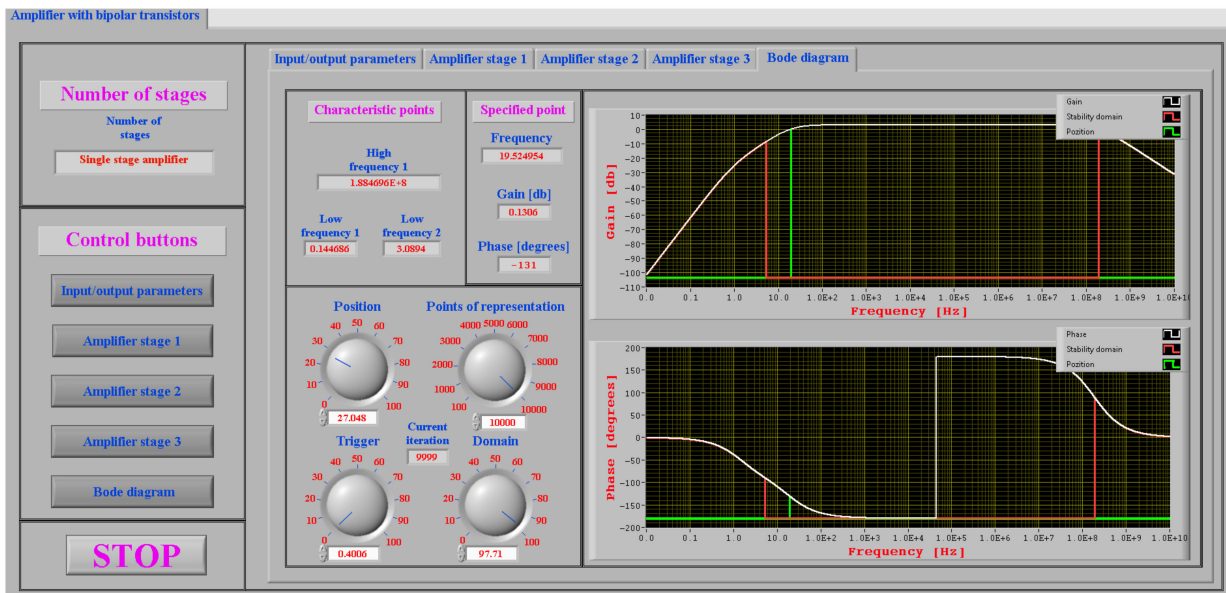
Figure 27. Bode diagram for line 4 from Table 1 with SW$_{CEe1}$ to OFF, for low cut frequency of 19.5 Hz.
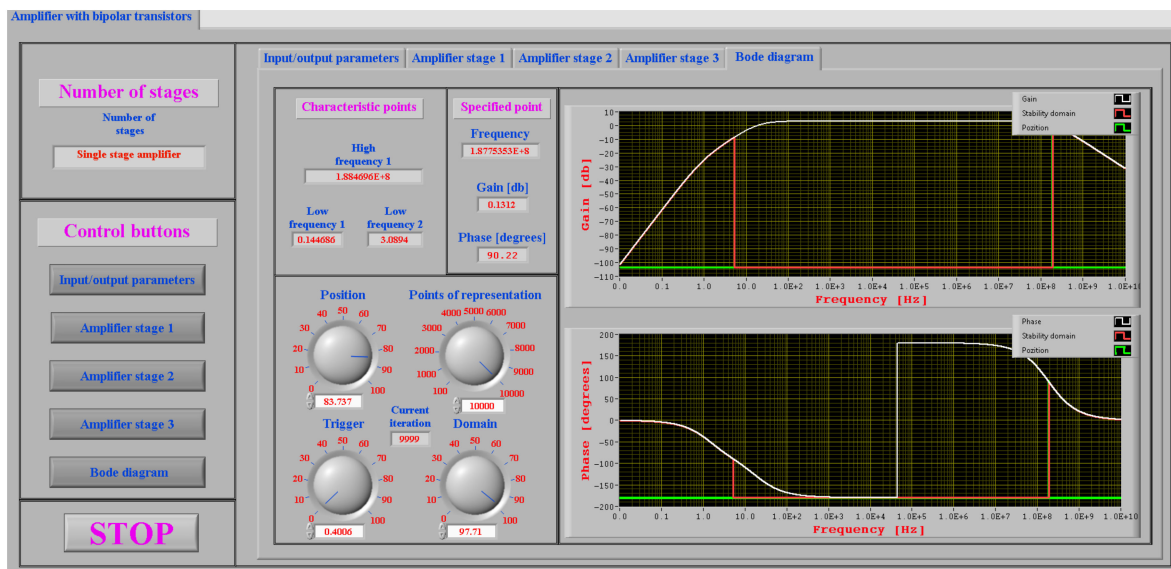

Figure 28. Bode diagram for line 4 from Table 1 with SW$_{CEe1}$ to OFF, for high cut frequency of 188.7 MHz.

As in the previous situation when SW$_{CEe1}$ was ON, a similar comparison between the simulations and experimental results can be made when SW$_{CEe1}$ was OFF. The comparison results can be seen in Figure 29.

Analyzing the gain diagram reveals that the simulation results are very similar at medium and high frequencies. At medium frequencies both simulations and measurements are very close.

In terms of the phase diagram, both simulations and measurements achieve similar values when crossing from $-180°$ to $180°$, and the LabVIEW simulations and measurements are nearly identical at medium frequencies.
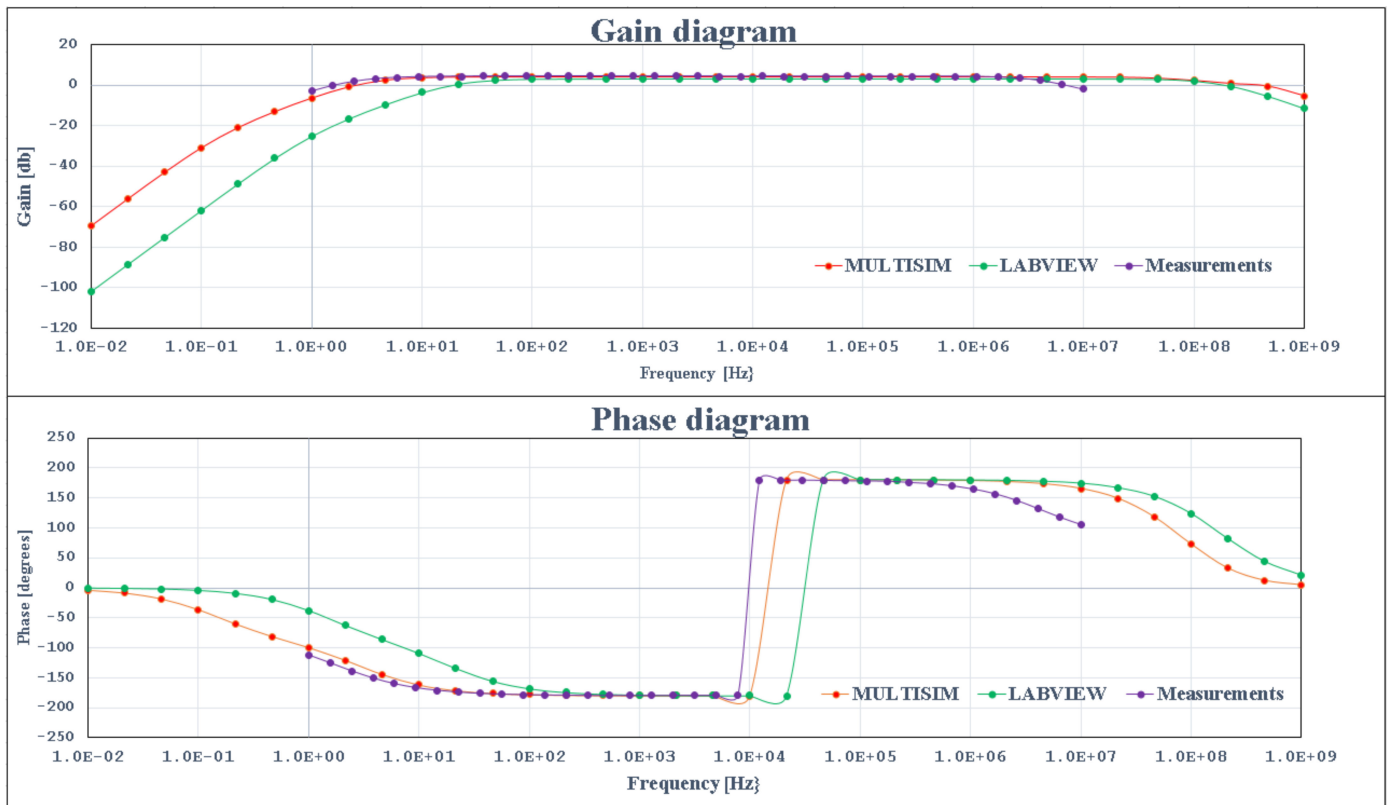
Figure 29. Simulations and experimental results for common emitter connection with SW_{CEe1} to OFF.

4.2. Simulation and Experimentation Results for Common Collector Connection

The input parameter values for this connection were chosen, like in the previous section, in such a way that the Bode diagram presented two different low pulsations [14–16]. These values are: for generator parameters, $R_g = 0.05$ kΩ and $e_g = 10$ mV; for load resistance, $Rs = 1$ kΩ; for coupling capacitors between the generator and the amplifier stage, $C_G = 10$ µF; and for coupling capacitors between amplifier stage and the load, $Cs = 10$ µF.

The parameter values for the common collector connection are presented in Figure 12.

As previously stated, the structure of an amplifier stage can be modified using the switches SW_{RGc1}, SW_{RB2c1} and SW_{RSc1}. Table 2 presents the values of the output parameters R_{Ic1}, A_{Uc1} and R_{Oc1} for all situations in which SW_{RGc1}, SW_{RB2c1} and SW_{RSc1} can be established.

Table 2. The values of the output parameters.

SW_{RGc1}	SW_{RB2c1}	SW_{RSc1}	R_{Ic1} [kΩ]	A_{Uc1}	R_{Oc1} [kΩ]
OFF	OFF	OFF	17.092	0.985	0.013
OFF	OFF	ON	16.815	0.980	0.013
OFF	ON	OFF	8.767	0.985	0.013
OFF	ON	ON	8.694	0.980	0.013
ON	**OFF**	**OFF**	**17.092**	**0.985**	**0.013**
ON	OFF	ON	16.815	0.980	0.013
ON	ON	OFF	8.767	0.985	0.013
ON	ON	ON	8.694	0.980	0.013

Table 2 reveals some conclusions regarding the effect of the three switches on the values of the output parameters.

1. Selecting the polarization mode of the transistor base with resistive divider by connecting switch SW_{RB2c1} in the ON state causes the input resistance R_{Ic1} to decrease.

2. None of the three switches have any effect on the A_{Uc1} value.

3. None of the three switches have any effect on the R_{Oc1} value.

Figures 30 and 31 show the Bode diagrams generated by simulations for the selected line from Table 2.
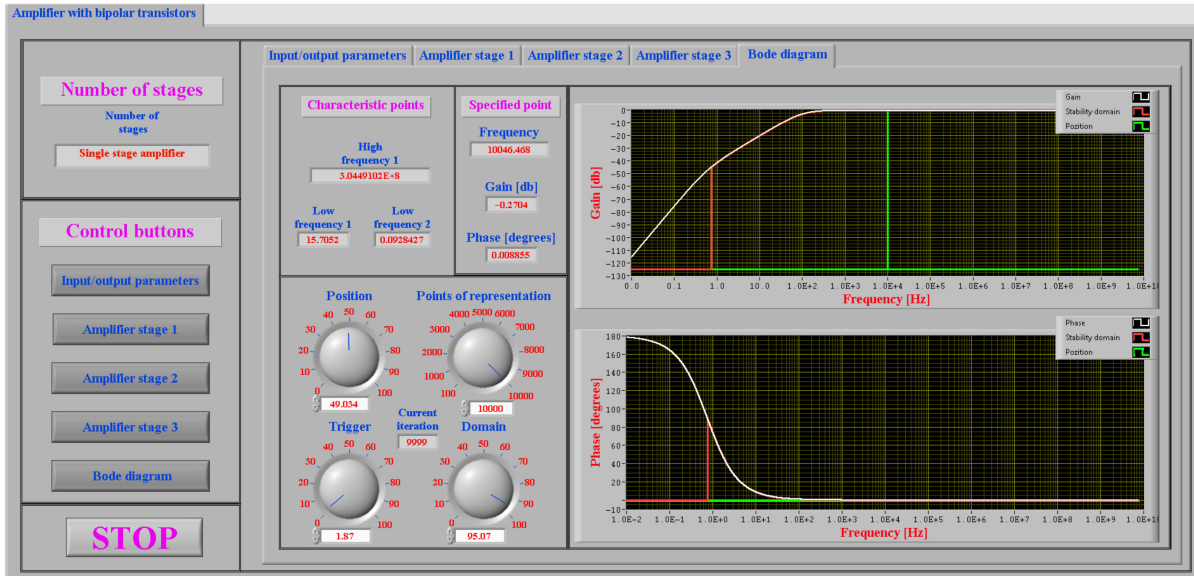

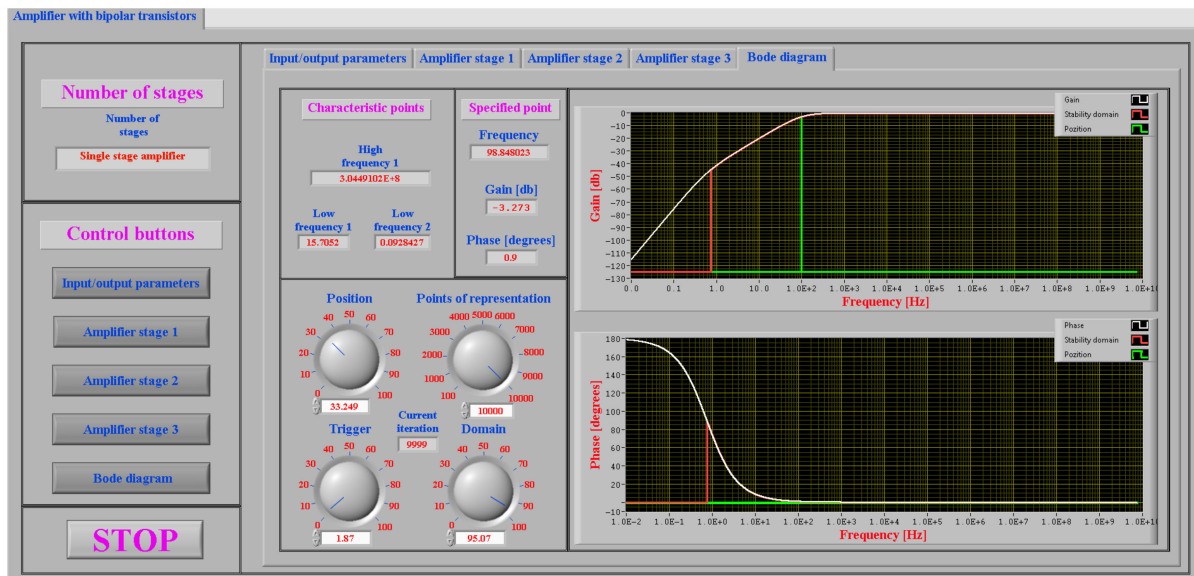**Figure 30.** Bode diagram for line 5 from Table 2, for 10 kHz frequency.

Figure 31. Bode diagram for line 5 from Table 2, for low cut pulsations of 98.85 Hz.

The simulation results for the common collector connection obtained with Multisim are shown in Figure 32.
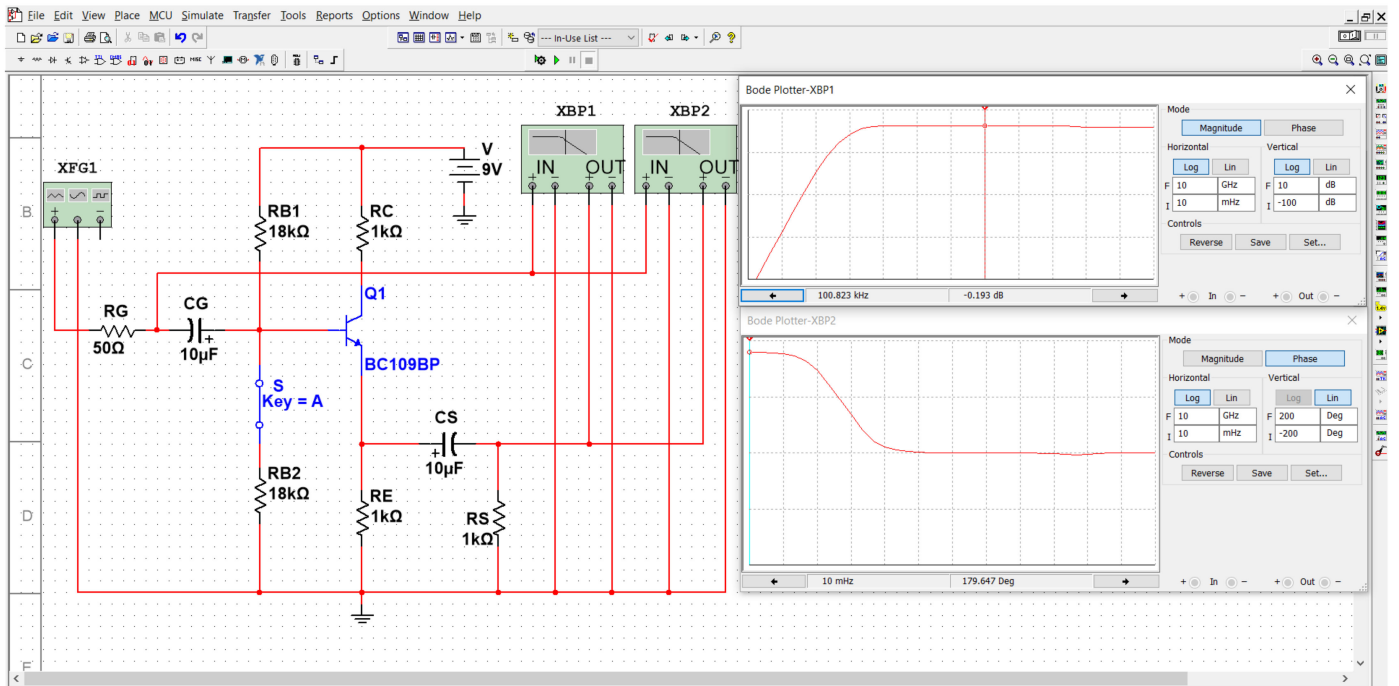
Figure 32. Simulation results for common collector connection, using Multisim.

Experimental measurements were performed on a real circuit using an Electronic Explorer Board, which can also be used to determine the Bode characteristics. The measurement results obtained with the Electronic Explorer Board are presented in Figure 33.
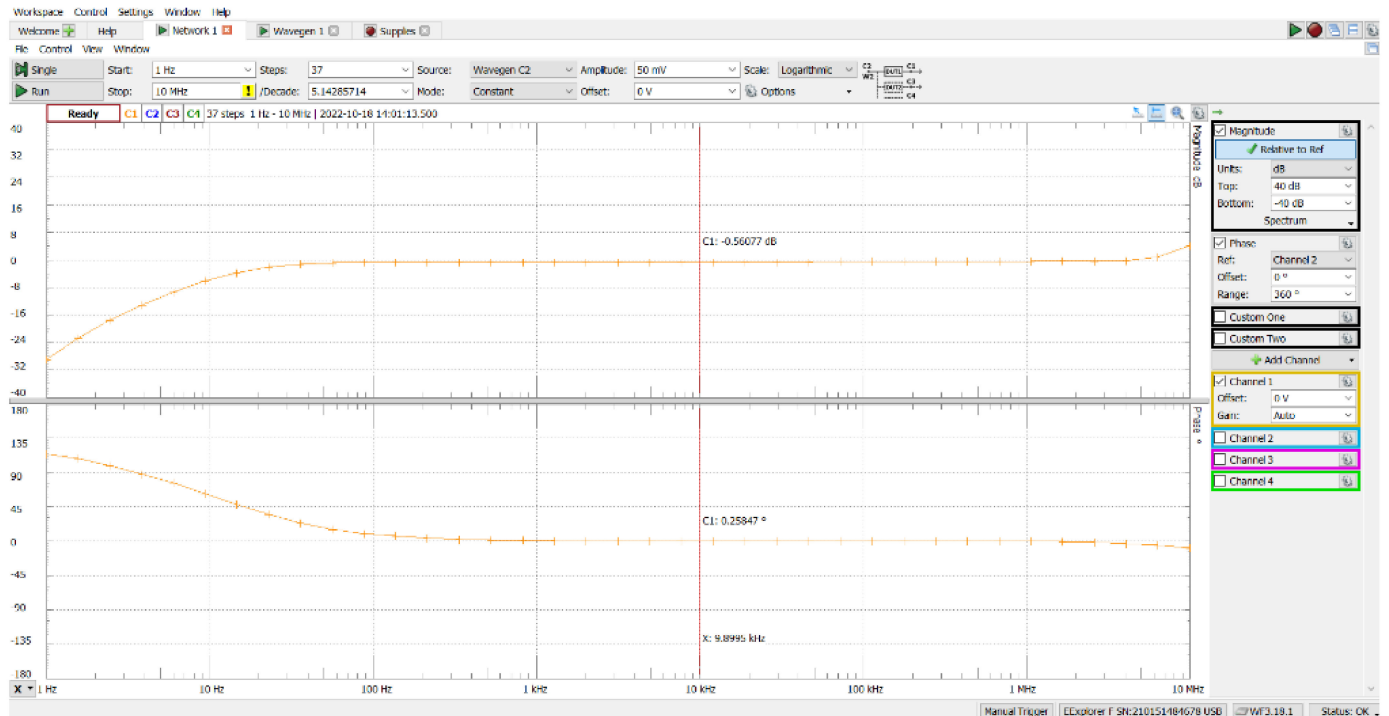

Figure 33. Measurement results for common collector connection, using Electronic Explorer Board.

A comparison between the simulations and experimental results can be seen in Figure 34.
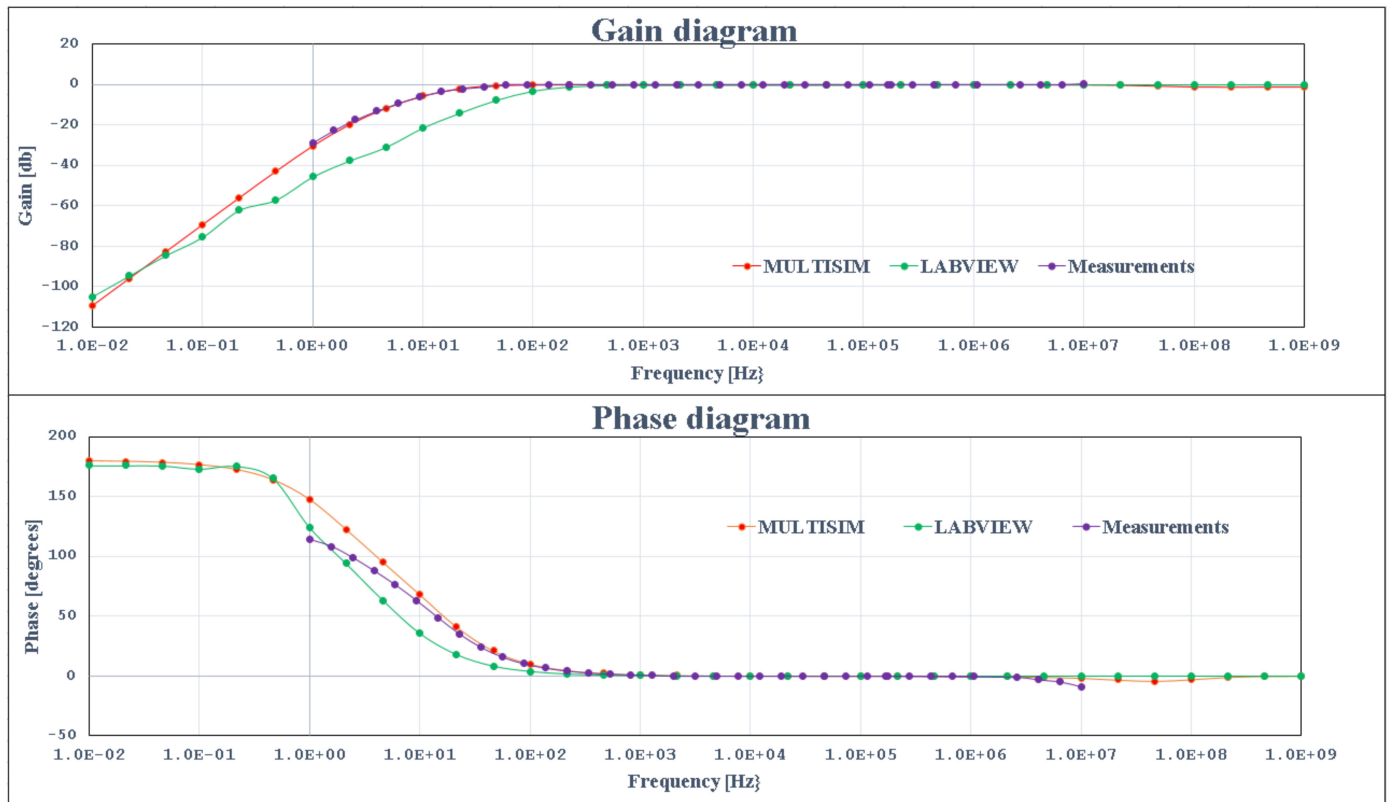
Figure 34. Simulations and experimental results for common collector connection.

Analyzing the gain diagram reveals that the simulation and experimental results are similar at all frequencies.

4.3. Simulation and Experimentation Results for Common Base Connection

The input parameter values for this connection were chosen, like in the previous sections, in such a way that the Bode diagram presented two different low pulsations [14–16]. These values are: for generator parameters, $R_g = 0.05$ kΩ and $e_g = 10$ mV; for load resistance, $R_s = 10$ kΩ; for coupling capacitors between the generator and the amplifier stage, $C_G = 1$ μF; and for coupling capacitors between amplifier stage and the load, $C_s = 100$ μF.

The parameter values for the common base connection are presented in Figure 15.

As previously stated, the structure of an amplifier stage can be modified using the switch SW_{RSb1}. Table 3 presents the values of the output parameters R_{Ib1}, A_{Ub1} and R_{Ob1} for the two situations in which SW_{RSb1} can be established.

Table 3. The values of the output parameters.

SW_{RSb1}	R_{Ib1} [kΩ]	A_{Ub1}	R_{Ob1} [kΩ]
OFF	**0.013**	**104.762**	**2.200**
ON	0.013	180.328	2.200

Table 3 reveals some conclusions regarding the effect of the switch SW_{RSb1} on the values of the output parameters.

1. The state of the switch SW_{RSb1} has no effect on the input resistance R_{Ib1} or the output resistance R_{Ob1}.

2. The ON state of switch SW_{RSb1} causes the A_{Ub1} value to increase.

Figures 35–37 show the Bode diagrams generated by simulations for the selected line from Table 3.
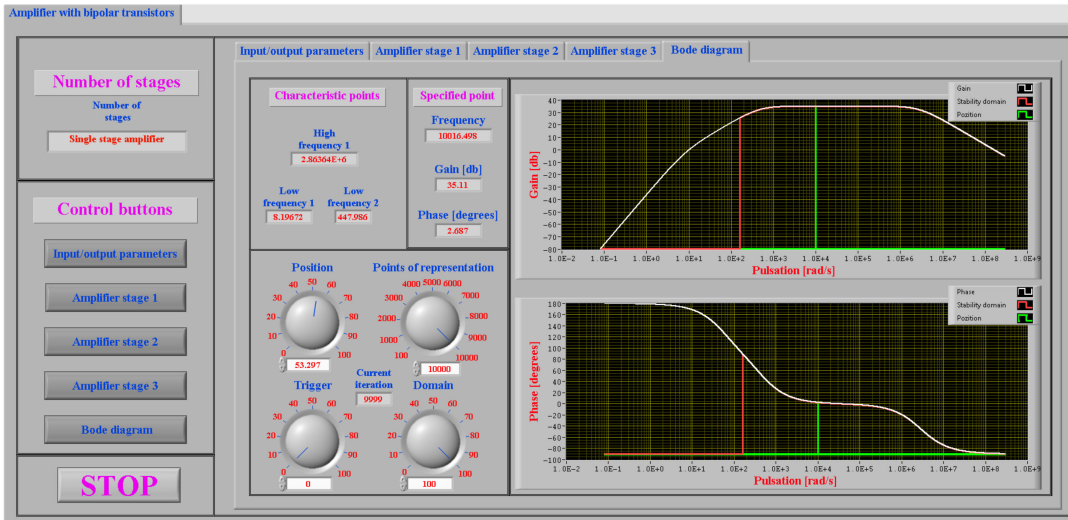
Figure 35. Bode diagram for line 1 from Table 3, for 10 kHz frequency.
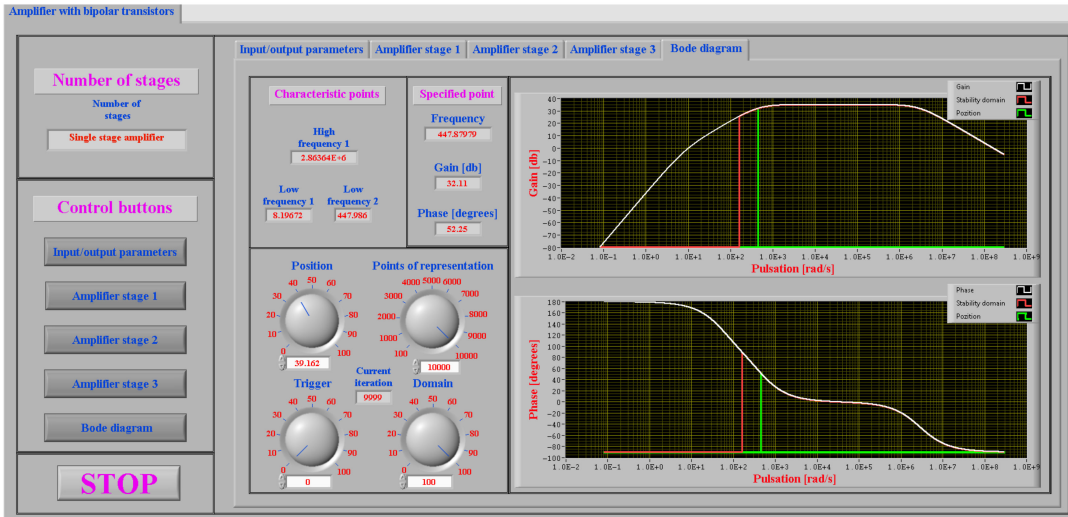
Figure 36. Bode diagram for line 1 from Table 3, for low cut pulsations of 447.9 Hz.
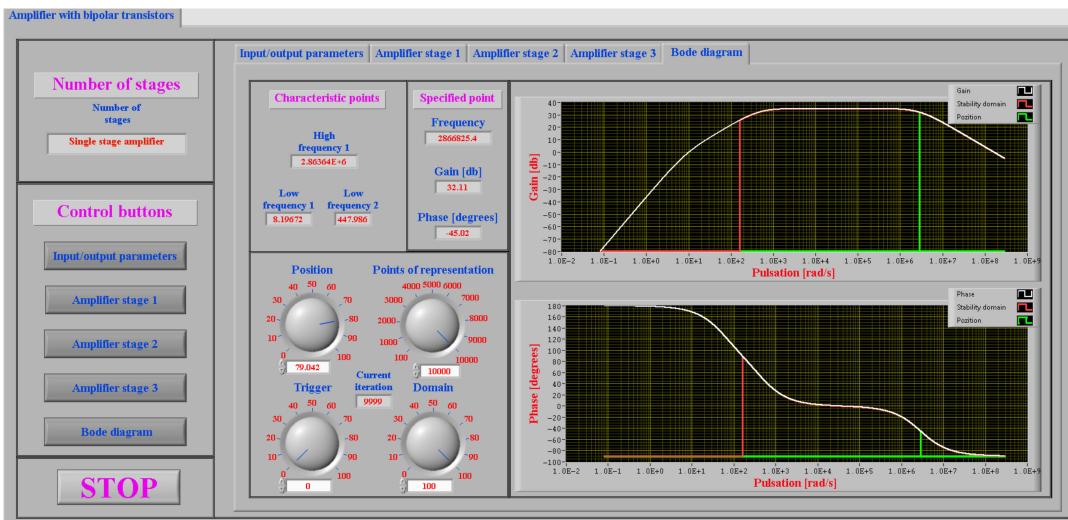
Figure 37. Bode diagram for line 1 from Table 3, for high cut pulsations of 2.86 MHz.

The simulation results obtained with Multisim are shown in Figure 38.
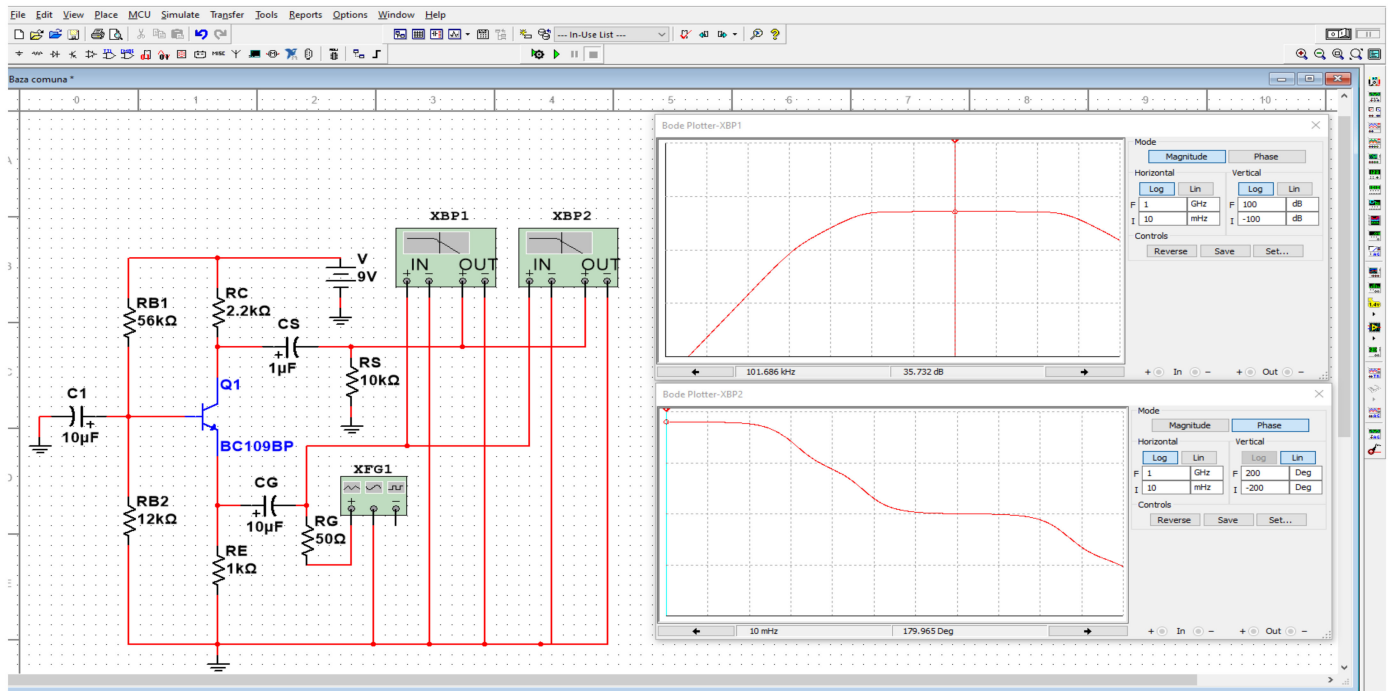
Figure 38. Simulation results for common base connection, using Multisim.

As with previous connections, to validate the simulation results produced by LabVIEW and Multisim, experimental measurements were performed on a real circuit using an Electronic Explorer Board.

The measurement results obtained with the Electronic Explorer Board are presented in Figure 39.

Figure 39. Measurement results for common base connection, using Electronic Explorer Board.

A comparison between the simulations and experimental results can be seen in Figure 40.

Figure 40. Simulations and experimental results for common base connection.

Analyzing the gain diagram reveals that the simulation and experimental results are similar at low and medium frequencies. At high frequencies the LabVIEW simulations and measurements are nearly identical.
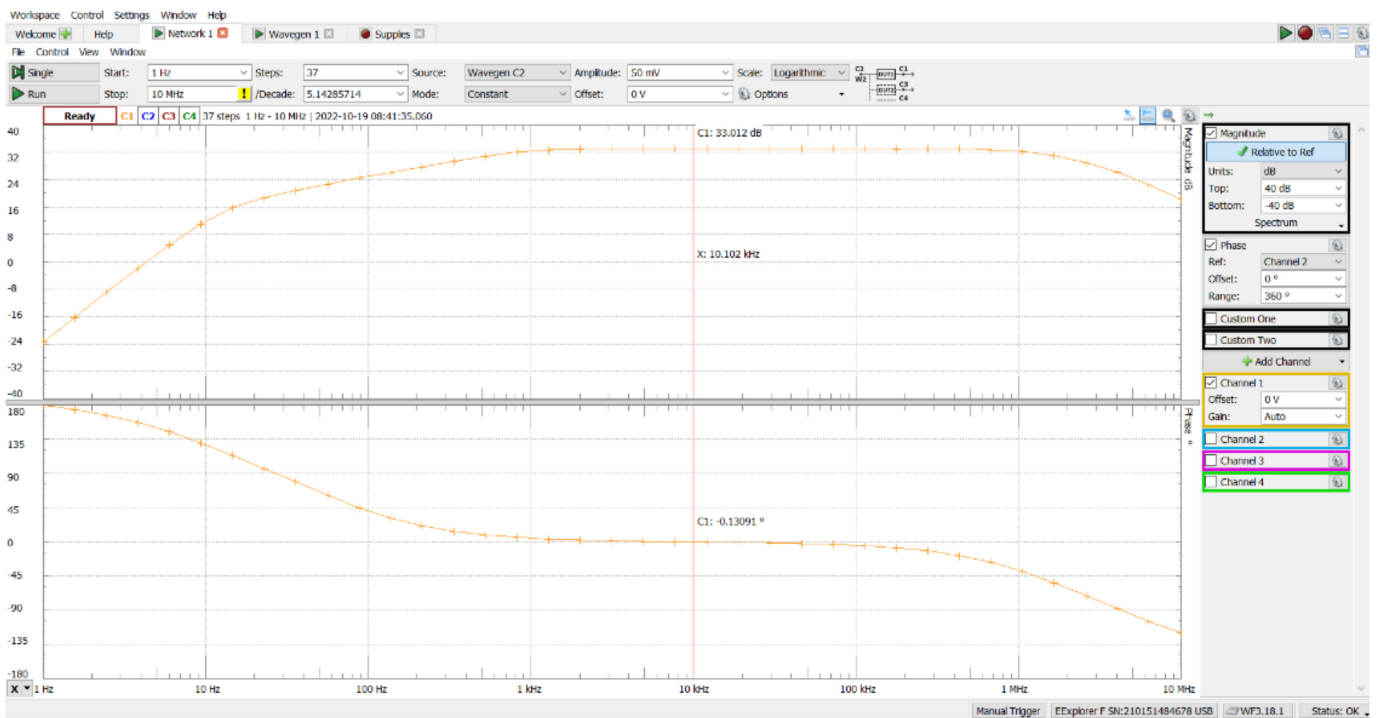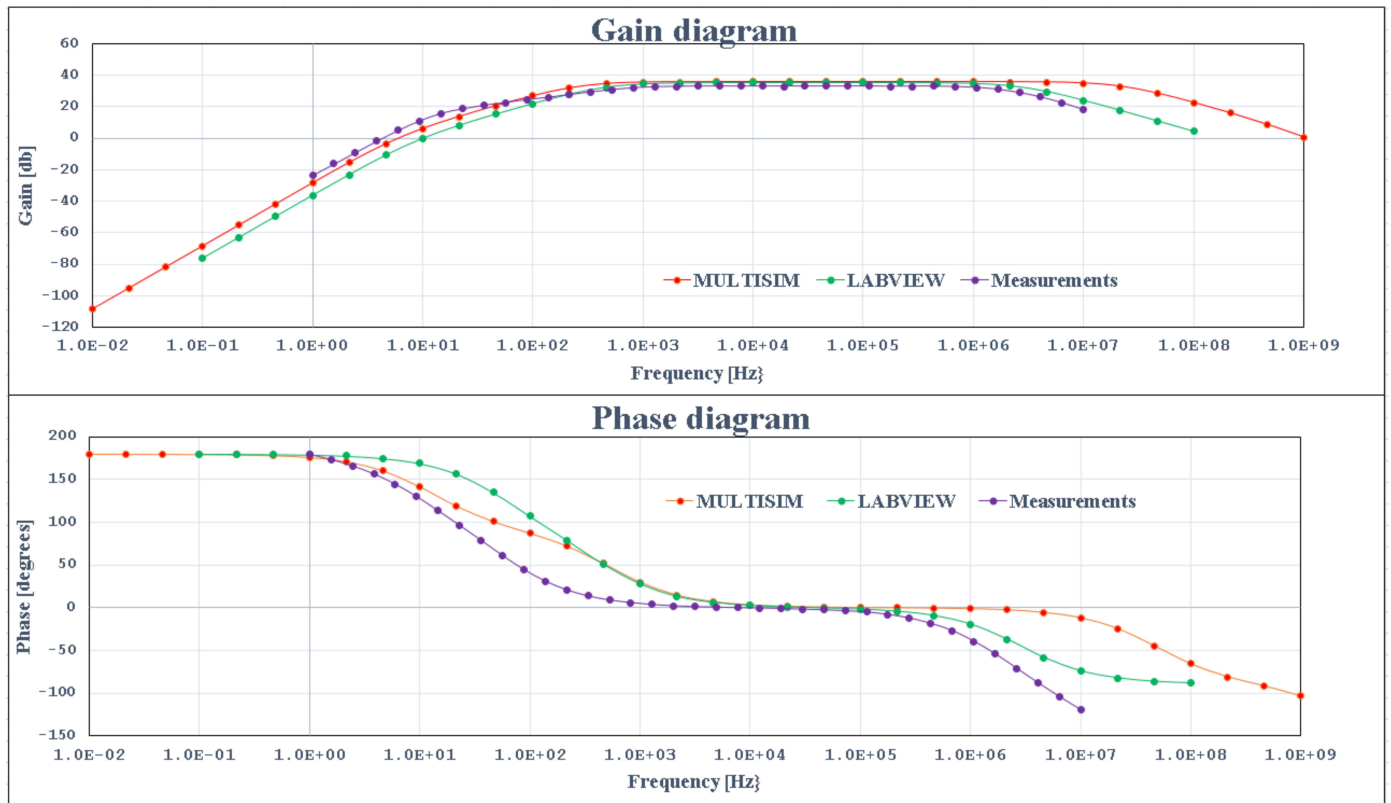
In terms of the phase diagram, both simulations and measurements have the same behavior from 180° to −180°.

5. Conclusions

The investigation of the functionality of an amplifier with discrete components in various connections is a complex process due to the large number of circuit elements whose values influence the amplifier's output parameters.

This paper describes a LabVIEW application that calculates the output parameters of a single-stage amplifier, such as input and output resistance, voltage amplification, and gain-frequency and phase-frequency Bode diagrams.

An amplifier stage can be studied in three different configurations: common emitter, common collector and common base. Different transistor polarisation possibilities can be selected for each connection. The application allows for the generation of various transistor polarization schemes by coupling some circuit elements with switches.

The amplifier's stability zone, as well as the gain and phase of the amplifier for a given frequency value, can be determined using Bode diagrams.

A specified single-stage amplifier can be designed by changing both the configuration of the amplifier and the value of any circuit element.

Because the application allows the visualization of the electronic scheme of each connection, the mathematical relations for determining the output parameters, and the dynamical scheme, it can be used for educational purposes.

In order to validate simulation results from the LabVIEW application, the specialized program Multisim was used, as well as experimental measurements using the Electronics Explorer Board. Both Multisim and the Electronics Explorer Board can determine Bode characteristics. In both simulation and experimental amplifiers, the same schemes with the same transistor were used.

This paper demonstrated that the LabVIEW application can produce similar simulation results to Multisim or measured results using the Electronics Explorer Board. The application described in this article is an innovative type of tool that may be used as a learning tool because it performs circuit analysis in simulation software and experimental comparisons.

Figures 25, 29 and 34 show that the Multisim, LabVIEW, and measurement characteristics are not identical, which is due to the use of a simplified version of the quadrupole model used in simulations.

In the future, the authors intend to develop this application for two and three stages as a first step, followed by a study of different global reaction configurations as a second step.

Author Contributions: Conceptualization, C.C. and C.P.; methodology, M.P.; software C.P. and C.C.; validation, I.B. and S.M.; writing—original draft preparation, M.P. and S.M.; writing—review and editing, C.C., C.P. and M.P. All authors have read and agreed to the published version of the manuscript.

Data Availability Statement: The raw data supporting the conclusions of this article will be made available by the authors on request.

Conflicts of Interest: The authors declare no conflict of interest.

Nomenclature

u_1	input quadrupole voltage
u_2	output quadrupole voltage
i_1	input quadrupole current
i_2	output quadrupole current
$h_{11}, h_{12}, h_{21}, h_{22}$	quadrupole "h" parameters
$h_{11e}, h_{12e}, h_{21e}, h_{22e}$	quadrupole "h" parameters in common emitter connection
$h_{11c}, h_{12c}, h_{21c}, h_{22c}$	quadrupole "h" parameters in common collector connection
$h_{11b}, h_{12b}, h_{21b}, h_{22b}$	quadrupole "h" parameters in common base connection
R_I, R_O	input and output resistance
R_{Ie1}, R_{Oe1}	input and output resistance in common emitter connection
R_{Ic1}, R_{Oc1}	input and output resistance in common collector connection
R_{Ib1}, R_{Ob1}	input and output resistance in common base connection
R_g	generator resistance
R_d	dynamic resistance
e_g	generator voltage
C_1, C_3	coupling capacitors
C_2	decupling capacitors
R_{B1}, R_{B2}	resistors connected on base
R_{B1e1}, R_{B2e1}	resistors connected on base in common emitter connection
R_{B1c1}, R_{B2c1}	resistors connected on base in common collector connection
R_{B1b1}, R_{B2b1}	resistors connected on base in common base connection
R_C	resistors connected on collector
R_{Ce1}	resistors connected on collector in common emitter connection
R_{Cc1}	resistors connected on collector in common collector connection
R_{Cb1}	resistors connected on collector in common base connection
R_E	resistors connected on emitter
R_{Ee1}	resistors connected on emitter in common emitter connection
R_{Ec1}	resistors connected on emitter in common collector connection
R_{Eb1}	resistors connected on emitter in common base connection

R_s	load resistor
Au	voltage amplification
A_{ue1}	voltage amplification in common emitter connection
A_{uc1}	voltage amplification in common collector connection
A_{ub1}	voltage amplification in common base connection
$R_{i,next}$, R_{IN}	input resistance of the next stage
$R_{o,prev}$	output resistance of the previous stage
C_G	coupling capacitors between the generator and the amplifier stage
C_S	coupling capacitors between the amplifier stage and the load
R_{i1}	input resistance
R_{o1}	output resistance
SW_{RSe1}, SW_{RB2e1}, SW_{CEe1}	used switches in common emitter connection
SW_{RSc1}, SW_{RB2c}, SW_{RGc1}	used switches in common collector connection
SW_{RSb1}	used switch in common base connection
F_{Tei1}	high cutting frequency transistor in common emitter connection
F_{Tci1}	high cutting frequency transistor in common collector connection
F_{Tbi1}	high cutting frequency transistor in common base connection
ω_1, ω_2	low cut pulsations of the stage
ω_{min}, ω_{max}	minimum and maximum pulsation domain
Δ_ω	graphic resolution of the pulsation axis
N	number of points represented

References

1. Thomas, L. Floyd. In *Electronic Devices*, 5th ed.; Prentice Hall, Inc.: Hoboken, NJ, USA, 1999.
2. Prasad, R. *Analog and Digital Electronic Circuits*; Springer: Berlin/Heidelberg, Germany, 2021.
3. Singh, S.; Agrawal, S. *Analog and Digital Electronics*; Dreamtech Press: Wiley, India, 2021.
4. Ciugudean, M. *Devices and Electronical Circuits*; Politechnics Publishing House: Timisoara, Romania, 1999.
5. Pasca, S.; Tomescu, N.; Sztojanov, I. *Analogical and Digital Electronics*; Albastra Publishing House: Timisoara, Romania, 2011.
6. Tian, T.; Na, A.; Zhao, X.M.; Zeng, L.N.; Tao, Y. System Design of AC Open-Loop Gain Measurement of Amplifier. *Appl. Mech. Mater.* **2013**, *333*, 475–476. [CrossRef]
7. Radhakrishnan, R.K.; Sukumarapillai, K.; Hashemian, R. A nullor approach to the design of analog circuits for a desirable performance. *Microelectron. J.* **2018**, *78*, 54–62. [CrossRef]
8. Jeschke, S.; Al-Zoubi, A.Y.; Pfeiffer, O.; Natho, N.; Nsour, J. Classroom-laboratory interaction in an electronic engineering course. In Proceedings of the International Conference on Innovations in Information Technology, Al Ain, United Arab Emirates, 16–18 December 2008; pp. 337–341.
9. Qin, G.X.; Wang, G.G.; Mc Caughan, L.; Ma, Z.Q. Superiority of common-base to common-emitter heterojunction bipolar transistors. *Appl. Phys. Lett.* **2010**, *97*, 133506. [CrossRef]
10. Rode, D.L. Output resistance of the common-emitter amplifier. *IEEE Trans. Electron Devices* **2005**, *52*, 2004–2008. [CrossRef]
11. Okamoto, K.; Fujita, J.; Ishikawa, M.; Hattori, T. Original amplifier using only emitter and base of a Si bipolar transistor. In Proceedings of the 2014 IEEE International Meeting for Future of Electron Devices Kansai (IMFEDK), Kyoto, Japan, 19–20 June 2014; pp. 1–2.
12. Jiang, N.Y.; Wang, G.G.; Ma, Z.Q. Analytical explanation of different RF characteristics exhibited with common-emitter and common-base bipolar transistors. In Proceedings of the 2004 Bipolar/BICMOS Circuits and Technology Meeting, Montreal, QC, Canada, 12–14 September 2004; pp. 112–115.
13. Narasimhamurthy, K.C.; Bindhu, T.S.; Natraj, S.; Bharath, G.C.; Vismithata, S.A.; Shiva, A. Exploration of Common Emitter Amplifier in Remote Lab. *Cyber-Phys. Syst. Digit. Twins* **2020**, *80*, 623–633.
14. Wakui, S. Relationship between parameter estimation method based on Bode diagram and co-quad diagram. *Int. J. Jpn. Soc. Precis. Eng.* **1997**, *31*, 227–231.
15. Hahn, J.; Edison, T.; Edgar, T.F. A note on stability analysis using Bode plots. *Chem. Eng. Educ.* **2001**, *35*, 208–211.
16. Fan, L.; Miao, Z. Admittance-Based Stability Analysis: Bode Plots, Nyquist Diagrams or Eigenvalue Analysis? *IEEE Trans. Power Syst.* **2020**, *35*, 3312–3315. [CrossRef]
17. Li, L. Design of Electronic Circuit Virtual Measurement System based on LabVIEW. *Agro Food Ind. Hi-Tech* **2017**, *28*, 2036–2040.
18. Huang, Z.; Wang, X. Development of virtual instrument motor experiment teaching system based on LabVIEW. *J. Chem. Pharm. Res.* **2014**, *6*, 1361–1368.
19. Xu, K.; Tao, Y. Circuit Analysis Courseware Design Based on LabVIEW. In Proceedings of the International Conference on Education Technology, Management and Humanities Science (ETMHS 2015), Shaanxi, China, 21–22 March 2015; Volume 27, pp. 991–995.
20. Peng, J.S. Integrated Simulation and Implementation Based on Multisim and LabVIEW. In Proceedings of the International Conference of China Communication (ICCC2010), Guangxi, China, 13–14 October 2010; pp. 295–297.

21. Hui, I.S. Design of virtual circuit experiment based on the LabVIEW. In Proceedings of the International Power, Electronics and Materials Engineering Conference (IPEMEC 2015), Dalian, China, 16–17 May 2015; Volume 17, pp. 1118–1121.
22. Li, Y.M.; Cai, B. Electronic Circuit Virtual Laboratory Based on LabVIEW and Multisim. In Proceedings of the 7th International Conference on Intelligent Computation Technology and Automation (ICICTA), Changsha, China, 25–26 October 2014; pp. 222–225.
23. Dominguez, M.A.; Fernandez, J.A.; Carrillo, J.M.; de la Vega, P.T.M. Remote Interactive Experiments Using LabVIEW for Electronic Test Bench. In Proceedings of the Inted2011: 5th International Technology, Education and Development Conference, Valencia, Spain, 7–9 March 2011; pp. 749–754.
24. Weihao, W.; Xiaoli, Q. Design of Electronic Virtual Experiment System Based on LabVIEW. *IOP Conf. Ser. Mater. Sci. Eng.* **2019**, *490*, 042024.
25. Wang, W.T.; Zhao, J.C.; Gu, Z.F.; Liu, Z. Application of LabVIEW in teaching of circuit analysis. *Exp. Sci. Technol.* **2014**, *12*, 49–51.
26. Piao, C.R. Design of the virtual instrument. *J. Nav. Univ. Eng.* **2006**, *6*, 82–85.
27. Calatrava, A.A.; Marcos, R.M.; Damian, J.S.Q. A Pilot Experience with Software Programming Environments as a Service for Teaching Activities. *Appl. Sci.* **2021**, *11*, 341. [CrossRef]
28. Richelli, A. Low-Voltage Integrated Circuits Design and Application. *Electronics* **2021**, *10*, 89. [CrossRef]
29. Hasan, S.; Abbas, Z.K.; Parvez, M.A. Equivalent Circuit Modeling of a Dual-Gate Graphene FET. *Electronics* **2021**, *10*, 63. [CrossRef]
30. Chung, D.; Woon, C.; Inyeob, J.; Joonhyeon, J. Design of Cut Off-Frequency Fixing Filters by Error Compensation of MAXFLAT FIR Filters. *Electronics* **2021**, *10*, 553. [CrossRef]
31. Urdaneta, P.; María, C.; Amaia, M.Z.; Ibon, O.R. Recommendation Systems for Education: Systematic Review. *Electronics* **2021**, *10*, 1611. [CrossRef]
32. Gürkan, S.; Karapınar, M.; Sorgunlu, H.; Öztürk, O.; Doğan, S. Development of a photovoltaic panel emulator and LabVIEW-based application platform. *Comput. Appl. Eng. Educ.* **2020**, *28*, 1291–1310. [CrossRef]
33. Allawi, F.M.A. Educational interactive LabVIEW simulations of field hydraulic conductivity tests below water table. *Comput. Appl. Eng. Educ.* **2021**, *29*, 1480–1488. [CrossRef]
34. Allawi, F.M.A. Educational interactive hydraulic and geometric design of a spillway using LabView and geometrical modeling. *Comput. Appl. Eng. Educ.* **2019**, *27*, 145–153. [CrossRef]
35. Allawi, F.M.A. Educational interactive vector simulation of water table control designs using LabView. *Comput. Appl. Eng. Educ.* **2020**, *28*, 853–866. [CrossRef]
36. Szávuly, M.I.; Tóos, Á.; Barabás, R.; Szilágyi, B. From modeling to virtual laboratory development of a continuous binary distillation column for engineering education using MATLAB and LabVIEW. *Comput. Appl. Eng. Educ.* **2019**, *27*, 1019–1029. [CrossRef]
37. RiveraOrtega, U. A simple LabVIEW-MATLAB implementation to observe the wavelength tunability of a laser diode with a diffraction grating. *Comput. Appl. Eng. Educ.* **2016**, *24*, 365–370. [CrossRef]